PHYSIOLOGY

Reducing the mitochondrial oxidative burden alleviates lipid-induced muscle insulin resistance in humans

Matteo Fiorenza[1,2]*, Johan Onslev[3], Carlos Henríquez-Olguín[3,4], Kaspar W. Persson[3], Sofie A. Hesselager[3], Thomas E. Jensen[3], Jørgen F. P. Wojtaszewski[3], Morten Hostrup[1], Jens Bangsbo[1]

Preclinical models suggest mitochondria-derived oxidative stress as an underlying cause of insulin resistance. However, it remains unknown whether this pathophysiological mechanism is conserved in humans. Here, we used an invasive in vivo mechanistic approach to interrogate muscle insulin action while selectively manipulating the mitochondrial redox state in humans. To this end, we conducted insulin clamp studies combining intravenous infusion of a lipid overload with intake of a mitochondria-targeted antioxidant (mitoquinone). Under lipid overload, selective modulation of mitochondrial redox state by mitoquinone enhanced insulin-stimulated glucose uptake in skeletal muscle. Mechanistically, mitoquinone did not affect canonical insulin signaling but augmented insulin-stimulated glucose transporter type 4 (GLUT4) translocation while reducing the mitochondrial oxidative burden under lipid oversupply. Complementary ex vivo studies in human muscle fibers exposed to high intracellular lipid levels revealed that mitoquinone improves features of mitochondrial bioenergetics, including diminished mitochondrial H_2O_2 emission. These findings provide translational and mechanistic evidence implicating mitochondrial oxidants in the development of lipid-induced muscle insulin resistance in humans.

INTRODUCTION

Insulin resistance is a main feature of obesity and type 2 diabetes. Skeletal muscle is the primary site of insulin-stimulated glucose uptake and thus the key tissue accounting for the impaired peripheral glucose disposal characterizing insulin-resistant states (*1*).

Nutrient overload is a prominent cause of insulin resistance (*2*). In particular, excess fat intake may induce insulin resistance within skeletal muscle through the accumulation of intramyocellular lipids, which ultimately suppress insulin signaling (*3*). Acquired or inherited mitochondrial dysfunction has been proposed as a nexus between lipid oversupply and muscle insulin resistance (*4*). Mechanistically, dysfunctional mitochondria may display a reduced capacity to oxidize lipids, resulting in accumulation of muscle lipid intermediates that disrupt insulin signaling (*5*). However, in contrast to such mitochondrial dysfunction theory of insulin resistance, genetic approaches that limit fatty acid uptake into muscle mitochondria, thereby inducing accumulation of cytosolic lipid intermediates, have been reported to improve whole-body glucose homeostasis (*6*–*9*), suggesting that insulin resistance arises from excessive rather than diminished mitochondrial fat oxidation. Hence, although the interplay between lipid oversupply, mitochondrial function, and insulin action remains controversial and incompletely understood (*10*–*12*), preclinical data support an intertwined relationship between lipid-induced insulin resistance and mitochondrial stress (*13*).

Mitochondria are a major source of superoxide and hydrogen peroxide [hereinafter referred to as reactive oxygen species (ROS)] (*14*). Excess ROS generation by mitochondria promotes a pro-oxidative shift in redox homeostasis leading to disrupted redox signaling and oxidative damage, i.e., oxidative stress (*15*), which contributes to the pathogenesis of insulin resistance and diabetes (*16*, *17*). Because mitochondrial ROS (mtROS) production rates increase markedly during fat oxidation (*18*–*21*), this led to the supposition that mitochondria-derived oxidative stress is the connecting link between lipid oversupply and insulin resistance (*13*, *22*). In support, recent evidence posits that increased mtROS resulting from coenzyme Q (CoQ) depletion is a driver of lipid-induced insulin resistance in skeletal muscle (*23*). Furthermore, independent of fat oxidation, mitochondrial oxidative stress may originate from the accumulation of cytosolic lipid intermediates, which, by inhibiting mitochondrial adenosine diphosphate (ADP) transport, induce an increase in mitochondrial membrane potential and superoxide production (*24*, *25*). Collectively, the intracellular stresses imposed by lipid oversupply appear to converge upon mitochondria (*26*, *27*), with mtROS likely acting as a critical signal in the cascade of events that impair insulin action. In support, genetic approaches to diminish mtROS have been proven to effectively counteract insulin resistance induced by a high-fat diet (HFD) in rodents (*28*–*31*). This suggests that strategies targeting the mitochondrial oxidative burden hold therapeutic potential against insulin resistance under obesogenic conditions.

Mitochondria-targeted antioxidants (mtAOs) are pharmacological compounds that selectively deliver antioxidant moieties to mitochondria by utilizing either the mitochondrial membrane potential or affinity to a mitochondrial component (*32*, *33*). Selective suppression of mtROS/oxidative damage with mtAO can preserve (*28*) or partly rescue (*34*) insulin action in HFD-fed rodents and convey greater metabolic benefits than suppression of non-mtROS (*34*).

Together, although preclinical data point toward a causative link between excess mtROS and insulin resistance (*35*), it remains unknown whether this pathophysiological mechanism is conserved in humans. In this regard, clinical trials have reported inconsistent effects of general antioxidants on insulin action and glycemic control (*36*); however, whether this is due to the unspecificity of general antioxidants to

[1]August Krogh Section for Human Physiology, Department of Nutrition, Exercise and Sports, University of Copenhagen, Copenhagen 2100, Denmark. [2]Department of Biomedical Sciences, University of Copenhagen, Copenhagen 2200, Denmark. [3]August Krogh Section for Molecular Physiology, Department of Nutrition, Exercise and Sports, University of Copenhagen, Copenhagen 2100, Denmark. [4]Exercise Science Laboratory, Faculty of Medicine, Universidad Finis Terrae, Santiago 1509, Chile.
*Corresponding author. Email: matteo.fiorenza@sund.ku.dk

mitochondrial redox state remains elusive. Furthermore, species-specific differences in metabolism may contribute to translational barriers between preclinical models and humans (*37*). Accordingly, human metabolic studies including selective targeting of mitochondrial redox state would be of high translational relevance and can help understand whether and how mtROS affect the molecular mechanisms controlling insulin action in humans, ultimately aiding the development of new therapeutic strategies to counter insulin resistance.

We therefore conducted a proof-of-concept translational trial integrating invasive in vivo experiments in humans and ex vivo/in vitro muscle studies to investigate the causal relationship between muscle mitochondrial redox state and insulin resistance while interrogating the underlying molecular mechanisms. Here, we show that selective reduction of the mitochondrial oxidative burden by the mtAO mitoquinone mitigates the impairments in muscle insulin sensitivity elicited by lipid oversupply and that this is associated with rescue of a component of the molecular machinery governing muscle insulin action along with improvements in mitochondrial bioenergetic function.

RESULTS

The mtAO mitoquinone ameliorates lipid-induced muscle insulin resistance in humans in vivo

To investigate the role of mtROS in human skeletal muscle insulin resistance, we developed an integrative experimental model combining intravenous infusion of a lipid emulsion and heparin with intake of the mtAO mitoquinone to pharmacologically manipulate mitochondrial redox state in vivo. Through simultaneous hyperinsulinemic clamp studies, we assessed insulin-dependent muscle glucose uptake by means of the femoral arteriovenous balance technique (Fig. 1, A and B). Lipid plus heparin infusion was used to acutely elevate plasma free fatty acid concentrations and progressively induce a lipotoxic environment in skeletal muscle, i.e., a metabolic state leading to insulin resistance (*38*, *39*) and increased mtROS production (*40*). To exacerbate the degree of insulin resistance and mitochondrial oxidative stress elicited by the lipid infusion, and thereby augment the potential salvage effect of the mtAO mitoquinone, our mechanistic approach was implemented in adult males with overweight and prediabetes (Table 1); a cohort that displays an insulin-resistant phenotype likely characterized by a preexisting state of lipid-induced mitochondrial stress (*41*, *42*).

Lipid infusion markedly elevated circulating free fatty acids (Fig. 1C) to an extent reported to impair muscle insulin sensitivity (*43*–*45*). The overall decrease in QUICKI observed after 3 hours of lipid infusion confirmed the detrimental effect of the lipid overload on insulin sensitivity (Fig. 1D).

To target the putative mitochondrial redox mechanisms underlying lipid-induced insulin resistance, capsules containing the mtAO mitoquinone or identical placebo capsules were orally administered before and during the lipid infusion in a randomized crossover fashion (figs. S1 and S2C). Intake of mitoquinone improved insulin action at the skeletal muscle level, as measured by the insulin-stimulated glucose uptake across the leg (Cohen's $d = 0.77$) (Fig. 1, F and G), and tended to improve whole-body insulin sensitivity, as apparent from the 30% greater SI_{clamp} compared with placebo ($d = 0.53$) (Fig. 1E). Notably, although a strong correlation was apparent between mitoquinone-induced changes in whole-body and muscle insulin sensitivity (Fig. 1L), the smaller improvement observed at the whole-body level may imply divergent effects of mitoquinone on liver and muscle insulin action.

The mitoquinone-mediated enhancement in muscle insulin sensitivity was associated with trends toward greater arteriovenous glucose difference ($d = 0.66$) and femoral artery blood flow ($d = 0.38$) as compared with placebo (Fig. 1, H to K). Thus, mitoquinone-dependent salvage of muscle glucose uptake was likely driven by increased peripheral glucose extraction in combination with enhanced glucose delivery through greater tissue perfusion. This increase in tissue perfusion aligns with previous observations of mtAO-induced improvements in vascular endothelial function (*46*, *47*), which is otherwise impaired by hyperlipidemia and may contribute to blunting the hyperemic response to insulin infusion (*48*, *49*).

Given the greater muscle glucose uptake elicited by mitoquinone under lipid overload, we next determined whether muscle substrate oxidation was affected. We observed that, albeit a tendency toward a higher $\dot{V}_{CO2}$ with mitoquinone (Fig. 2A), neither muscle glucose nor lipid oxidation rates, as estimated by leg-specific indirect calorimetry (*50*), were influenced by mitoquinone (Fig. 2, B to D). While recognizing limitations of indirect calorimetry techniques, our findings agree with the proposed dissociation between muscle insulin resistance and mitochondrial substrate oxidation (*51*). To further interrogate the metabolic fate of glucose, we quantified lactate release across the leg, which has previously been shown to increase in response to lipid infusion (*43*, *44*). Leg lactate release was unaffected by mitoquinone (Fig. 2, E and F), supporting the lack of effects on substrate oxidation, and ultimately implying that mitoquinone improved muscle insulin sensitivity irrespective of increments in glucose oxidation.

Together, these data indicate that selective targeting of mitochondrial redox state with mitoquinone mitigated lipid-induced insulin resistance in human skeletal muscle in vivo, with this salvaging effect possibly driven by a synergistic increase in muscle glucose extraction and muscle tissue perfusion without apparent alterations in muscle substrate oxidation.

The mtAO mitoquinone does not affect canonical insulin signaling but enhances insulin-dependent GLUT4 translocation under lipid overload

Contrasting data have accumulated regarding the role of insulin signaling in lipid-induced insulin resistance. While some studies show impairments in proximal components of the insulin signaling pathway (*52*–*55*), others report intact insulin signaling (*43*, *44*, *56*–*59*). To elucidate whether the observed insulin-sensitizing action of mitoquinone under lipid stress was associated with improved insulin signaling, we assessed the phosphorylation of key proteins in the proximal and distal segments of the insulin signaling pathway (Fig. 3A). We found that proximal insulin signaling at the level of Akt2 was unaffected by mitoquinone (Fig. 3B), which is in contrast with the greater Akt phosphorylation observed during a glucose challenge in HFD-fed rodents treated with the mtAO SS-31 (*28*). Likewise, distal insulin signaling, as measured by the phosphorylation of the Akt substrates GSK3 and TBC1D4, was unaffected by mitoquinone (Fig. 3, C and D).

In light of preclinical data indicating that mitochondrial oxidative stress induces insulin resistance by impairing insulin-stimulated trafficking of glucose transporter type 4 (GLUT4) rather than canonical insulin signaling (*30*, *35*), we measured GLUT4 protein abundance in plasma membrane fractions (Fig. 3F) as a proxy of GLUT4 translocation (*60*). Insulin-mediated increments in sarcolemmal GLUT4 were apparent only with mitoquinone intake, which was associated with a greater sarcolemmal GLUT4 abundance than placebo (Fig. 3E). As

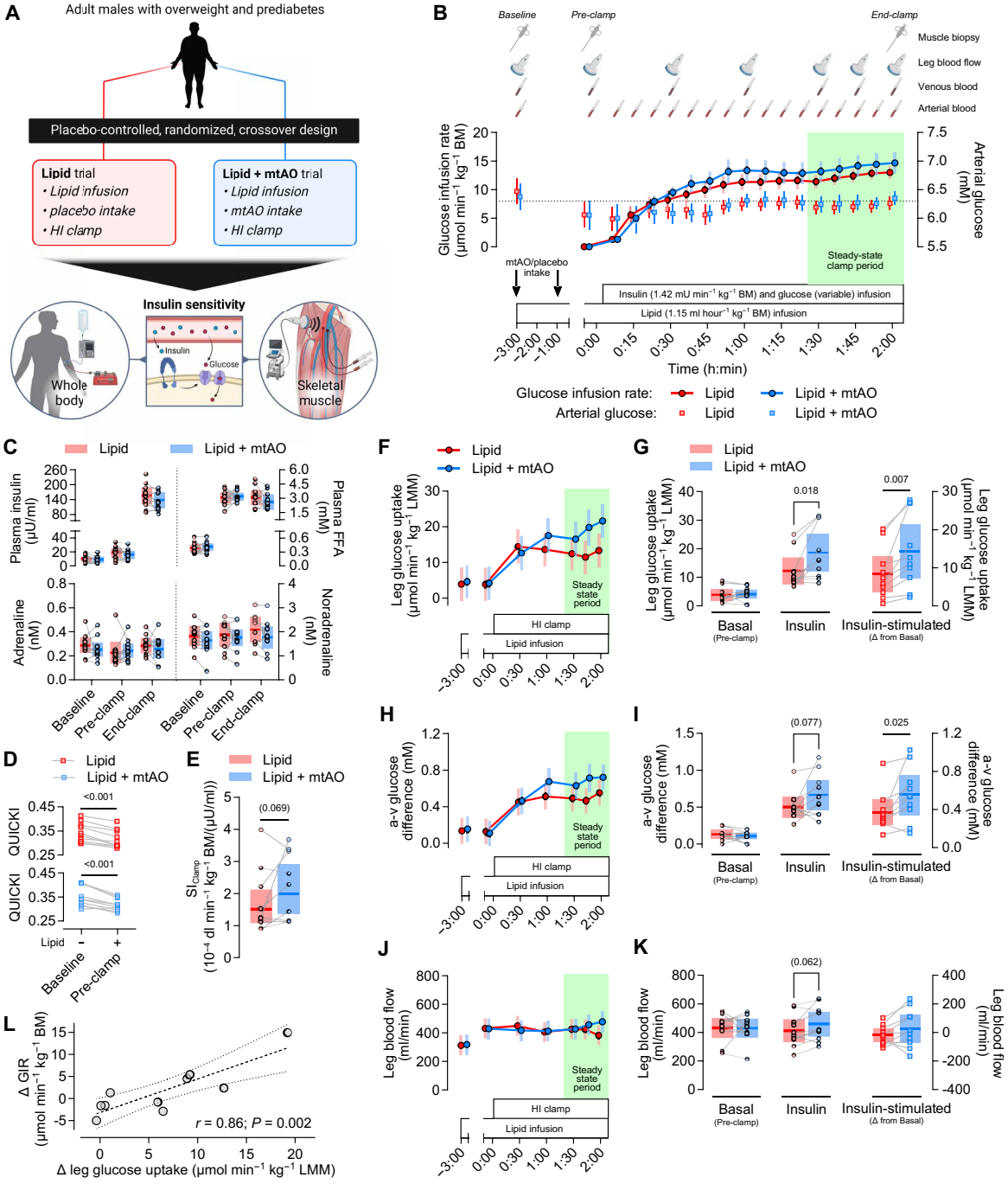

Fig. 1. The mtAO mitoquinone ameliorates lipid-induced muscle insulin resistance in humans in vivo. (**A**) Schematic overview of the study design. HI clamp, hyperinsulinemic-isoglycemic clamp. (**B**) Experimental trial workflow, including the mean glucose infusion rate corrected per body mass (BM) and the arterial glucose concentrations. The dotted line indicates arterial glucose concentration corresponding to isoglycemia. Data presented as means ± SEM. (**C**) Plasma insulin, free fatty acid (FFA), and catecholamine levels measured before the lipid infusion (Baseline), as well as before (Pre-clamp) and after (End-clamp) the HI clamp. Lipid + mtAO, $n = 9$ (End-clamp). (**D**) Individual changes in the quantitative insulin sensitivity check index (QUICKI) in response to 3 hours of lipid infusion. (**E**) Whole-body insulin sensitivity expressed as the clamp-derived index of insulin sensitivity (SI_{clamp}) (*122*). Lipid, $n = 10$; Lipid + mtAO, $n = 9$. (**F** to **K**) Skeletal muscle insulin sensitivity expressed as the leg glucose uptake, as calculated from the arteriovenous difference in plasma glucose concentration and the femoral arterial blood flow corrected per leg muscle mass (LMM). [(F), (H), and (J)] Time course of leg glucose uptake, a-v glucose difference, and leg blood flow. [(G), (I), and (K)] Leg glucose uptake, a-v glucose difference, and leg blood flow before the HI clamp (Basal) and during the steady-state clamp period (Insulin). Between-treatment differences in insulin-stimulated leg glucose uptake, a-v glucose difference, and leg blood flow, calculated as the change (Δ) from the basal to the steady-state clamp period. (**L**) Pearson's correlation between mtAO-induced changes (Δ) in glucose infusion rate (GIR) and leg glucose uptake. Linear mixed models were used to estimate between-treatment differences [(C), (E), (G), (I), and (K)]. Data presented as observed individual values with estimated means ±95% confidence limits, unless otherwise stated. $n = 10$, unless otherwise stated. Illustrations in (A) were created with BioRender.com.

Table 1. Participant characteristics. Data are means ± SD. HOMA2-IR, homeostatic model assessment of insulin resistance 2 (*123*); QUICKI, quantitative insulin sensitivity check index (*122*); HDL/LDL, high-/low-density lipoprotein; $\dot{V}_{O2max}$, maximal oxygen uptake.

Characteristics	Mean ± SD
Age (years)	51.5 ± 5.6
Height (m)	1.80 ± 0.06
Body mass (kg)	103.0 ± 16.2
Body mass index (kg/m^2)	31.7 ± 3.3
Body composition	
Fat-free mass (kg)	62.0 ± 7.2
Fat mass (kg)	37.3 ± 10.0
Percent body fat (%)	37.2 ± 5.0
Visceral fat mass (g)	2952 ± 739
Experimental leg muscle mass (kg)	8.96 ± 1.32
Fasting blood plasma parameters	
Glucose (mM)	5.9 ± 0.6
Hemoglobin A1c (%)	5.8 ± 0.4
Insulin (pM)	126 ± 43
Insulin C-peptide (pM)	1154 ± 250
HOMA2-IR	2.70 ± 0.64
QUICKI	0.308 ± 0.019
Total cholesterol (mM)	5.7 ± 1.1
HDL cholesterol (mM)	1.11 ± 0.22
LDL cholesterol (mM)	3.93 ± 0.80
Triglycerides (mM)	2.42 ± 0.96
Alanine aminotransferase (U/liter)	33.8 ± 2.5
Systolic blood pressure (mmHg)	128 ± 8
Diastolic blood pressure (mmHg)	84 ± 5
$\dot{V}_{O2max}$ (ml min^{-1} kg^{-1})	30.6 ± 5.0

changes in sarcolemmal GLUT4 were relatively small compared with the changes in muscle glucose uptake observed in vivo (Fig. 3G), we conducted a series of experiments in vitro to further interrogate the role of mtROS in GLUT4 translocation. First, we assessed the effect of mitoquinone on GLUT4 translocation in L6 muscle cells expressing a *myc*-tagged GLUT4 (Fig. 4A) and confirmed that mitoquinone rescues a lipid-induced GLUT4 translocation defect elicited by palmitate treatment (Fig. 4B). This suggests that mtROS are necessary for lipid-induced impairments in GLUT4 trafficking. Next, using a genetically encoded biosensor GLUT4-7*myc*-GFP construct in mouse muscle (*61*) (Fig. 4C), we demonstrated that treatment with the mitochondria-targeted pro-oxidant Mito-Paraquat (MitoPQ) impairs insulin-mediated GLUT4 translocation (Fig. 4D), revealing that mtROS induce GLUT4-dependent insulin resistance in mature skeletal muscle.

Collectively, these findings indicate that selective targeting of mitochondrial redox state with mitoquinone does not affect canonical insulin signaling but enhances insulin-stimulated GLUT4 trafficking in human skeletal muscle under lipid stress and that a pro-oxidative shift in mitochondrial redox state is sufficient to disrupt GLUT4 translocation in skeletal muscle.

The mtAO mitoquinone reduces the mitochondrial oxidative burden under lipid overload

To verify the link between the insulin-sensitizing and antioxidant action of mitoquinone under lipid stress, we measured markers of subcellular redox state in muscle biopsy samples obtained before initiation of the lipid infusion (Baseline) and upon termination of the HI clamp (End-clamp) (Fig. 5A). Cytosolic and mitochondrial redox state were assessed by measuring peroxiredoxin 2 (PRDX2) and peroxiredoxin 3 (PRDX3) dimerization, respectively (*62*). We found that, while the relative abundance of PRDX2 dimers was unchanged (Fig. 5B), mitoquinone intake was associated with lower PRDX3 dimerization at the end of the HI clamp (Fig. 5C), indicating a reduced mitochondrial oxidative burden compared with placebo. These findings support the compartmentalized action of mitoquinone and are consistent with preclinical data showing that the mitochondria-targeted pro-oxidant MitoPQ promotes dimerization of muscle PRDX3 without affecting PRDX2 redox state (*35*).

To further characterize alterations in muscle redox state, we quantified the abundance of oxidized/hyperoxidized peroxiredoxin (PRDX-$SO_{2/3}$) dimers, i.e., an indicator of overall peroxiredoxin oxidation (*63*, *64*), which tended to be lower with mitoquinone than with placebo (Fig. 5D). In addition, given that mitoquinone exerts its main antioxidant action by preventing lipid peroxidation within the inner mitochondrial membrane (*32*), we determined the abundance of the lipid peroxidation product 4-hydroxynonenal (4-HNE) in whole-muscle homogenates. We found that, although mitoquinone intake was associated with a decrease in muscle 4-HNE from baseline, this did not correspond with lower 4-HNE levels compared with placebo (Fig. 5E). This finding is consistent with data showing a lack of acute mitoquinone-dependent effects on blood lipid hydroperoxides (*65*) and possibly relates to the selective action of mitoquinone on mitochondrial lipids, which constitute only a fraction of the myocellular lipidome and may, therefore, be overlooked when measuring lipid peroxidation at the whole-muscle level.

Notably, none of the readouts of muscle oxidative stress appeared elevated following the 5-hour lipid infusion (Fig. 5, B to E). This observation is in contrast with the increased skeletal muscle oxidative burden (as measured by the ratio of reduced to oxidized glutathione) reported upon an oral lipid overload (*28*) and may be explained by the hyperinsulinemic state accompanying the lipid infusion in our study. Low-dose insulin has been reported to suppress ROS generation in human mononuclear cells (*66*) and to exert an inhibitory action on oxidative stress in patients with diabetes (*67*). Furthermore, insulin acutely improves muscle mitochondrial ADP sensitivity, a key determinant of redox state, in mice fed an HFD (*68*). Last, given that hyperinsulinemia per se may reduce systemic oxidative stress during hyperglycemic clamp conditions (*69*), it is conceivable that the high-dose insulin infusion used in the present study exerted an antioxidant action that abrogated lipid-induced increments in muscle oxidative stress.

To further interrogate the causal link between lipid overload and muscle mitochondrial oxidative stress, we conducted complementary studies in human muscle cells treated with palmitate (Fig. 5G). Exposure of primary human myotubes to 250 μM palmitate, i.e., the same levels impairing GLUT4 translocation in L6 muscle cells, induced an increase in PRDX3 dimerization as opposed to no changes in PRDX2 dimerization (Fig. 5H), thus corroborating the assumption that lipid

stress promotes mitochondrial, but not cytosolic, oxidative stress in human skeletal muscle.

Altogether, these data indicate that the mtAO mitoquinone reduced the mitochondrial oxidative burden in human skeletal muscle under lipid overload, whose intrinsic pro-oxidant action likely was blunted by the concomitant hyperinsulinemic state.

The mtAO mitoquinone improves muscle mitochondrial bioenergetics under lipotoxic conditions

To interrogate the purported relieving action of the mtAO mitoquinone on lipid-induced mitochondrial stress, we performed ex vivo analyses of mitochondrial bioenergetics in muscle biopsy specimen sampled from participants before initiating lipid infusion (Baseline). Our focus was specifically on muscle mitochondrial bioenergetic features known to be influenced by lipid stress and concurrently associated with insulin resistance (*24*, *25*). To this end, experiments were conducted under varying intramyocellular lipid concentrations, both with and without preexposure to mitoquinone (Fig. 6, A and B). Specifically, we used either 20 or 60 μM palmitoyl-CoA (P-CoA), the long-chain fatty acid derived from palmitate, to model a normal and a high intramyocellular lipid environment, respectively (*25*); with the higher P-CoA concentration being indicative of insulin resistance in humans (*70*). Given the absence of L-carnitine, which is required for CPT1-dependent transport of P-CoA into the mitochondrial matrix, we studied lipid-induced mitochondrial stress driven by cytosolic lipid accumulation rather than accelerated fat oxidation. Cytosolic P-CoA, apart from promoting ROS generation via inhibition of mitochondrial ADP transport (*24*), has amphiphilic properties that may alter the mitochondrial structure and cause peroxidation of the mitochondrial membrane (*71*, *72*), modifications that are supposedly prevented by the main antioxidant action of the mtAO mitoquinone.

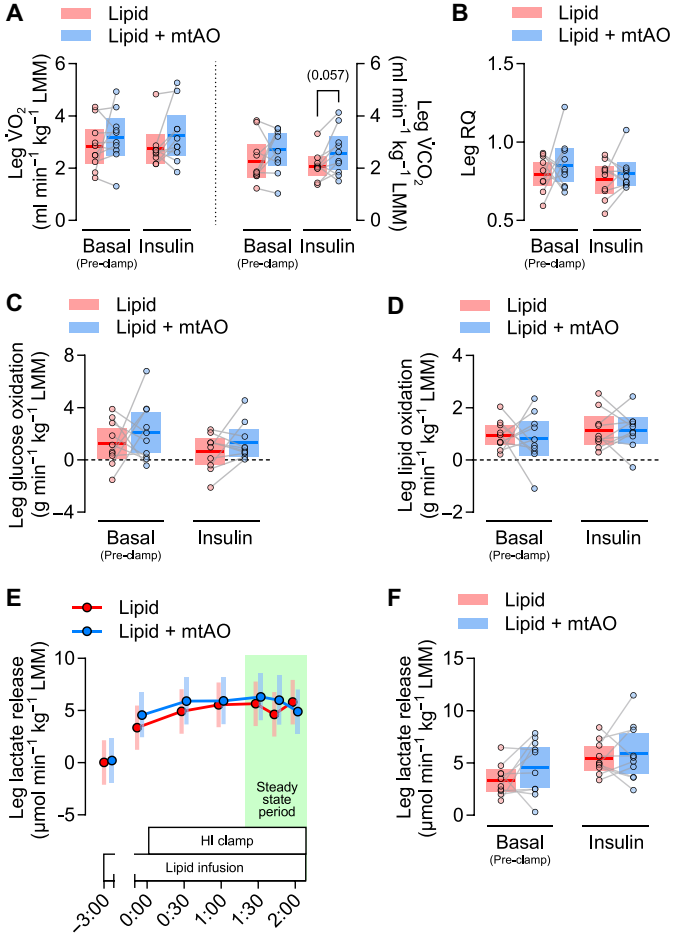

Fig. 2. The mtAO mitoquinone does not affect muscle substrate oxidation or lactate release under lipid overload. (**A** and **B**) Leg O_2 consumption ($\dot{V}O_2$), CO_2 release ($\dot{V}CO_2$), and respiratory quotient (RQ) before the hyperinsulinemic-isoglycemic (HI) clamp (Basal) and during the steady-state clamp period (Insulin). (**C** and **D**) Glucose and lipid oxidation across the leg, as estimated from the leg $\dot{V}O_2$ and $\dot{V}CO_2$, before the HI clamp (Basal) and during the steady-state clamp period (Insulin). (**E** and **F**) Leg lactate release as calculated from the arteriovenous difference in plasma lactate concentration and the femoral arterial blood flow. (E) Time course of leg lactate release (data are estimated means ±95% confidence limits). (F) Leg lactate release before the HI clamp (Basal) and during the steady-state clamp period (Insulin). Linear mixed models were used to estimate between-treatment differences [(A), (B), (C), (D), and (F)]. Data presented as observed individual values with estimated means ±95% confidence limits, unless otherwise stated. $n = 10$.

We found that mitochondrial maximal oxidative phosphorylation (OXPHOS) capacity was impaired under lipid stress and was not restored by mitoquinone, whereas the leak respiratory state associated with OXPHOS ($LEAK_{Omy}$) was unaffected by either lipid stress or mtAO (Fig. 6D). In contrast, mitoquinone partly attenuated lipid stress–induced impairments in an index of OXPHOS efficiency (Fig. 6D); mechanistically, this may be due to mitoquinone-mediated changes in CoQ redox state, which, by affecting mitochondrial supercomplex organization, can indirectly influence mitochondrial energy efficiency (*73*). Notably, mitochondrial respiration appeared highly heterogeneous in the present cohort, which aligns with the large interindividual variability in muscle mitochondrial content, as determined by citrate synthase activity (Fig. 6C).

Regarding mtROS, we observed that, under conditions that stimulate maximal mtROS production (i.e., saturating concentrations of succinate in the absence of ADP), mitochondrial H_2O_2 emission rates were unaffected by either lipid stress or mitoquinone (Fig. 6F). In contrast, under more physiological conditions stimulating submaximal ROS production (i.e., in the presence of ADP levels reflecting skeletal muscle at rest), we found that mitochondrial H_2O_2 emission rates were increased by lipid stress and that these increments were ablated by mitoquinone (Fig. 6F). Accordingly, the effectiveness of mitoquinone in preventing excessive mitochondrial H_2O_2 emission in skeletal muscle was apparent only when the in vitro environment resembled the in vivo muscle milieu.

As mitochondrial OXPHOS dysfunction and excessive ROS production may arise from impaired sensitivity of mitochondria to ADP (*25*), we also assessed whether lipid stress or mitoquinone altered such a feature of mitochondrial function. We found that the sensitivity of mitochondrial respiration (i.e., O_2 consumption rate) to ADP was impaired under lipid stress and was not ameliorated by mitoquinone, matching prior clinical (*24*) and preclinical data (*25*, *74*) (Fig. 6E). On the other hand, mitoquinone restored the ability of ADP to suppress mitochondrial H_2O_2 emission, which was otherwise impaired under lipid stress (Fig. 6G), a finding consistent with the beneficial effect of the mtAO SS-31 on the defective ADP sensitivity displayed by aging mouse muscle (*75*).

Together, these data demonstrate that impairments in muscle mitochondrial bioenergetics under lipid stress were partly rescued

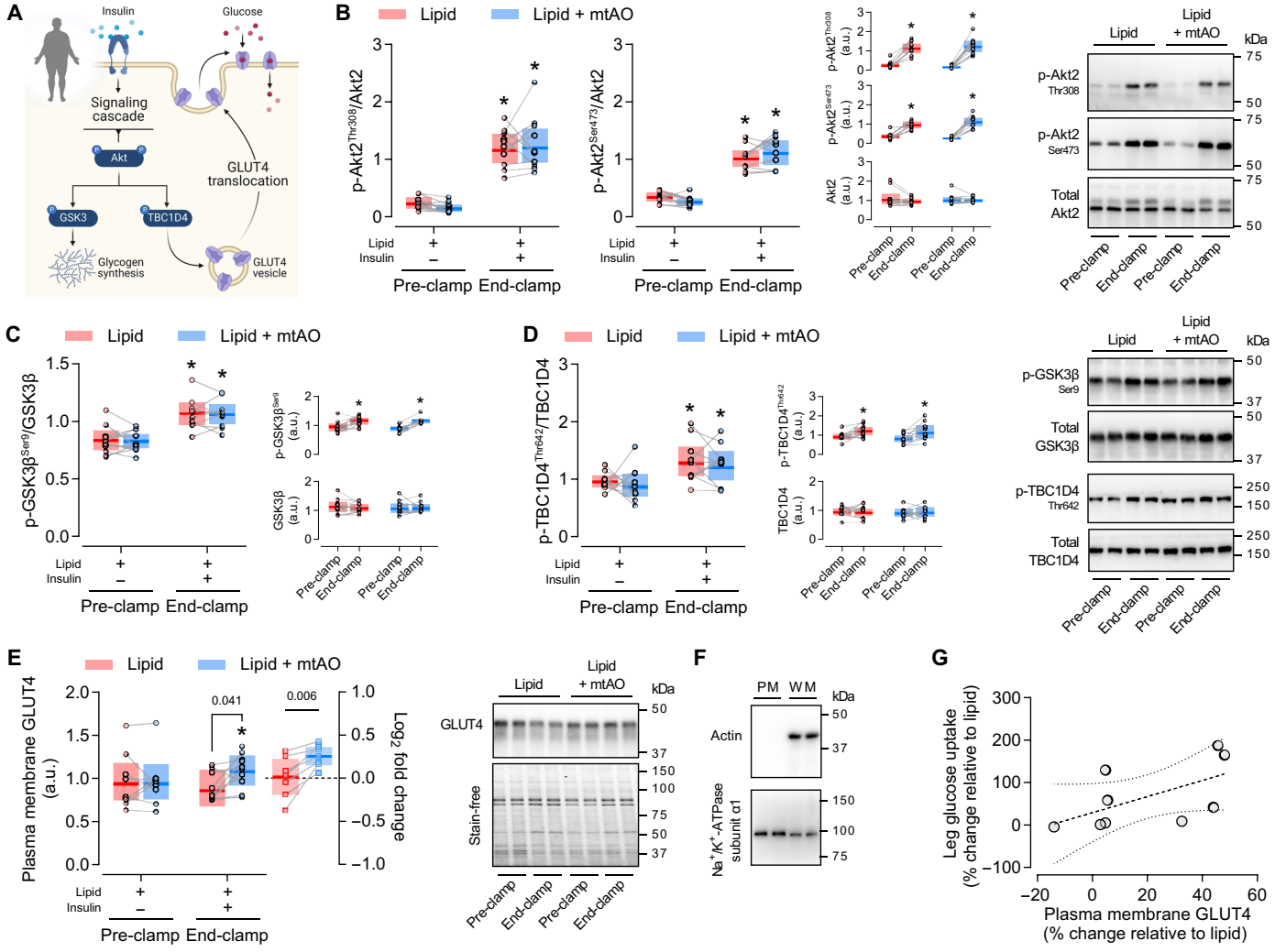

Fig. 3. The mtAO mitoquinone does not affect canonical insulin signaling but enhances insulin-dependent GLUT4 translocation under lipid overload. (**A**) Schematic overview of the major signaling events modulating insulin-stimulated glucose uptake in human skeletal muscle. (**B**) Proximal insulin signaling, as determined by phosphorylation of Akt2 on Thr308 and Ser473 in whole-muscle homogenates. (**C** and **D**) Distal insulin signaling, as determined by phosphorylation of the Akt substrates GSK3β on Ser9 (C) and TBC1D4 on Thr642 (D) in whole-muscle homogenates. (**E**) GLUT4 translocation, as determined by GLUT4 protein abundance in plasma membrane protein fractions. In-gel stain-free technology was used as a loading control. Lipid, $n = 8$ (Pre-clamp) and $n = 9$ (End-clamp); Lipid + mtAO, $n = 10$. Representative blots ($n = 2$ biological replicates from each muscle biopsy sample for each patient). (**F**) Purity of the isolated plasma membrane protein fractions (used to determine GLUT4 translocation), as determined by immunoblot analysis of actin (cytosolic protein marker) and Na^+/K^+-ATPase subunit α1 (plasma membrane protein marker) in plasma membrane homogenates (PM) as compared with the corresponding whole-muscle homogenates (WM). PM and WM samples were obtained by pooling a given volume of each individual sample. (**G**) Pearson's correlation between mtAO-induced changes in plasma membrane GLUT4 and leg glucose uptake under insulin stimulation. $n = 9$. Data [(B) to (E)] presented as observed individual values with estimated means ±95% confidence limits. Linear mixed models were used to estimate within- and between-treatment differences at End-clamp [(B) to (E)]. *Different from Pre-clamp ($P < 0.05$). $n = 10$, unless otherwise stated. Illustrations in (A) were created with BioRender.com.

by the mtAO mitoquinone. This was particularly evident in the rate of mtROS emitted under experimental conditions resembling the in vivo metabolic environment of skeletal muscle at rest.

DISCUSSION

Building on preclinical data suggesting a causal role of excess mtROS in the etiology of muscle insulin resistance, we conducted a mechanistic study to interrogate whether this pathophysiological mechanism translates to humans. By integrating pharmacological manipulation of mitochondrial redox state in vivo with simultaneous assessments of insulin-dependent glucose uptake into skeletal muscle, we demonstrated that selective reduction of the mitochondrial oxidative burden by intake of the mtAO mitoquinone enhances muscle insulin sensitivity under lipid stress (Fig. 7). This occurred in the absence of changes in canonical insulin signaling but in the presence of augmented insulin-mediated GLUT4 translocation, the mitochondrial redox-dependent modulation of which was confirmed by complementary studies in rodent muscle cells and muscle fibers. These results provide proof of principle that a pro-oxidative shift in mitochondrial redox state contributes to lipid-induced muscle insulin resistance in humans and suggest that disrupted GLUT4 trafficking

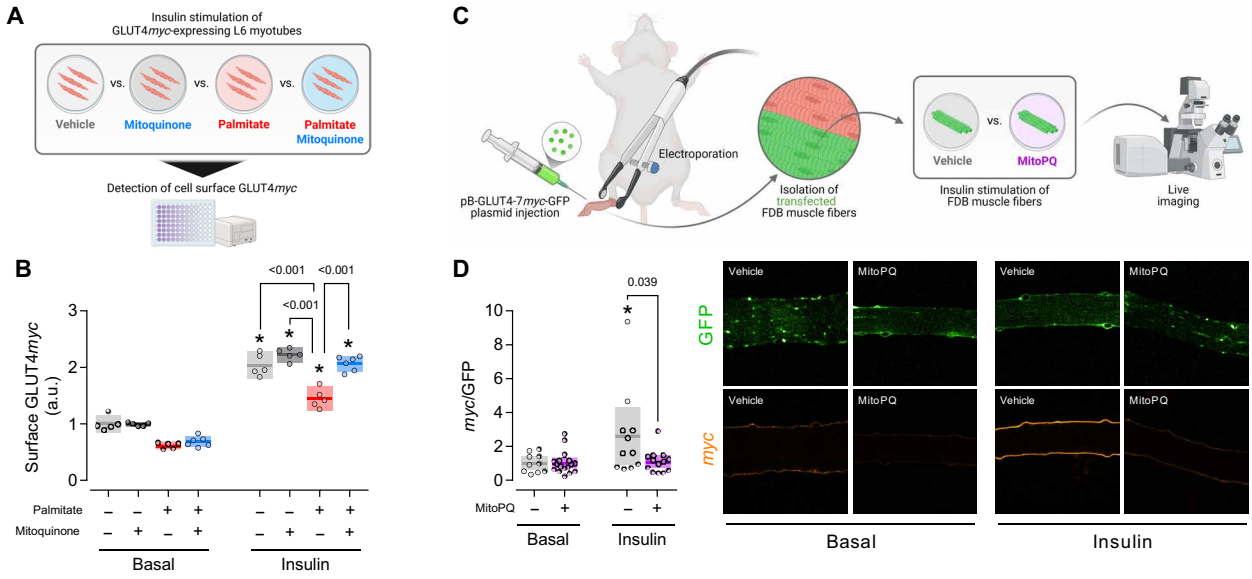

Fig. 4. The mtAO mitoquinone rescues palmitate-induced impairments in GLUT4 trafficking during insulin stimulation. (**A**) Workflow to determine insulin-stimulated GLUT4 translocation in L6 myotubes. (**B**) Insulin-stimulated GLUT4 translocation in L6 myotubes treated with either vehicle BSA (basal, $n = 5$; insulin, $n = 5$), 50 nM mitoquinone (basal, $n = 5$; insulin, $n = 5$), 250 μM palmitate (basal, $n = 5$; insulin, $n = 5$), or 250 μM palmitate + 50 nM mitoquinone (basal, $n = 6$; insulin, $n = 6$). Values are normalized to vehicle at basal. (**C**) Workflow to determine insulin-stimulated GLUT4 translocation in mouse FDB muscle fibers. (**D**) Insulin-stimulated GLUT4 translocation in mouse muscle fibers treated with either vehicle 0.1% ethanol (basal, $n = 10$; insulin, $n = 11$) or 10 μM MitoPQ (basal, $n = 17$; insulin, $n = 13$). Fibers were pooled from three mice. Values are normalized to vehicle at basal. Data presented as observed values with means ±95% confidence limits. A one-way ANOVA was used to estimate between-treatment differences. *Different from "Basal" ($P < 0.05$). Illustrations in (A) and (C) were created with BioRender.com.

is a molecular mechanism by which mtROS affect insulin-stimulated glucose disposal.

In addition, through ex vivo experiments, we showed that a high-lipid environment impairs features of mitochondrial bioenergetics in human muscle fibers and revealed that mitoquinone prevents lipid-induced increments in mtROS emission. These findings not only provide a comprehensive insight into the mitochondrial bioenergetic functions affected by lipid stress in human skeletal muscle but also demonstrate the effectiveness of mitoquinone in preserving some of these functions.

Our results contrast with the proposed irrelevance of mtROS in the pathophysiology of muscle insulin resistance in humans (*76*) and support findings from a seminal human intervention study inferring a connection between mitochondrial oxidative stress and lipid-induced insulin resistance (*28*). Specifically, Anderson *et al.* (*28*) showed that muscle mtROS production acutely increases upon an oral lipid overload. However, albeit accompanied by elegant rodent experiments, this observation did not allow to establish a causal relationship between lipid-induced mtROS and insulin resistance in humans. Our model addresses this translational gap by incorporating insulin clamp-based measurements of muscle insulin action with intravenous infusion of a fat emulsion combined with mtAO intake, a mechanistic approach that has a number of methodological advantages. First, by applying the femoral arteriovenous balance technique to the gold standard insulin clamp technique, we were able to determine leg muscle–specific insulin sensitivity in vivo. Second, the use of intravenous instead of oral lipid overload enabled the induction of lipid stress without involving the gastrointestinal tract (*77*), thus overcoming the insulinotropic effect of incretin hormones. Last, because lipid stress affects a multitude of mitochondrial mechanisms beyond redox homeostasis, the combination of mtAO intake with the intravenous lipid infusion permitted selective targeting of mitochondrial redox state.

The finding that lipid-induced insulin resistance was ameliorated by the mtAO mitoquinone matches preclinical studies showing that genetic approaches to enhance mtROS scavenging capacity can rescue insulin action under HFD feeding (*28*, *78*–*81*). In contrast, data from our human model partly contradict another preclinical study indicating that overexpression of mitochondria-targeted catalase (mCAT; a mitochondrial H_2O_2-specific scavenger) did not protect against insulin resistance in the acute lipid infusion model as opposed to the long-term HFD model of lipid overload (*31*). This may be related not only to the markedly higher degree of lipid stress imposed by the acute lipid infusion in our human model as compared with the mCAT mouse model (i.e., eightfold versus threefold increase in circulating free fatty acids) (*31*), but also to the differential mechanisms whereby mCAT and the mtAO mitoquinone exert their antioxidant action.

With respect to the metabolic benefits elicited by mitoquinone under lipid stress, our results align with those from studies in HFD-fed mice, where glycemic control and glucose metabolism were improved by long-term mitoquinone treatment (*34*, *82*–*86*). On the other hand, evidence supporting the metabolic health-enhancing effects of mitoquinone in humans is scarce and limited to studies in metabolically healthy individuals, where long-term treatment did not elicit significant enhancements in glycemic control indexes (*47*, *87*). However, it is noteworthy that the present results were obtained in an acute hyperlipidemic-hyperinsulinemic state that does not reflect normo-physiological conditions, implying that the favorable effects of mitoquinone on insulin action and glucose homeostasis may be apparent only in a setting of marked lipid-induced mitochondrial stress.

Skeletal muscle glucose uptake accounts for the vast majority of whole-body insulin-stimulated glucose disposal. Thus, under

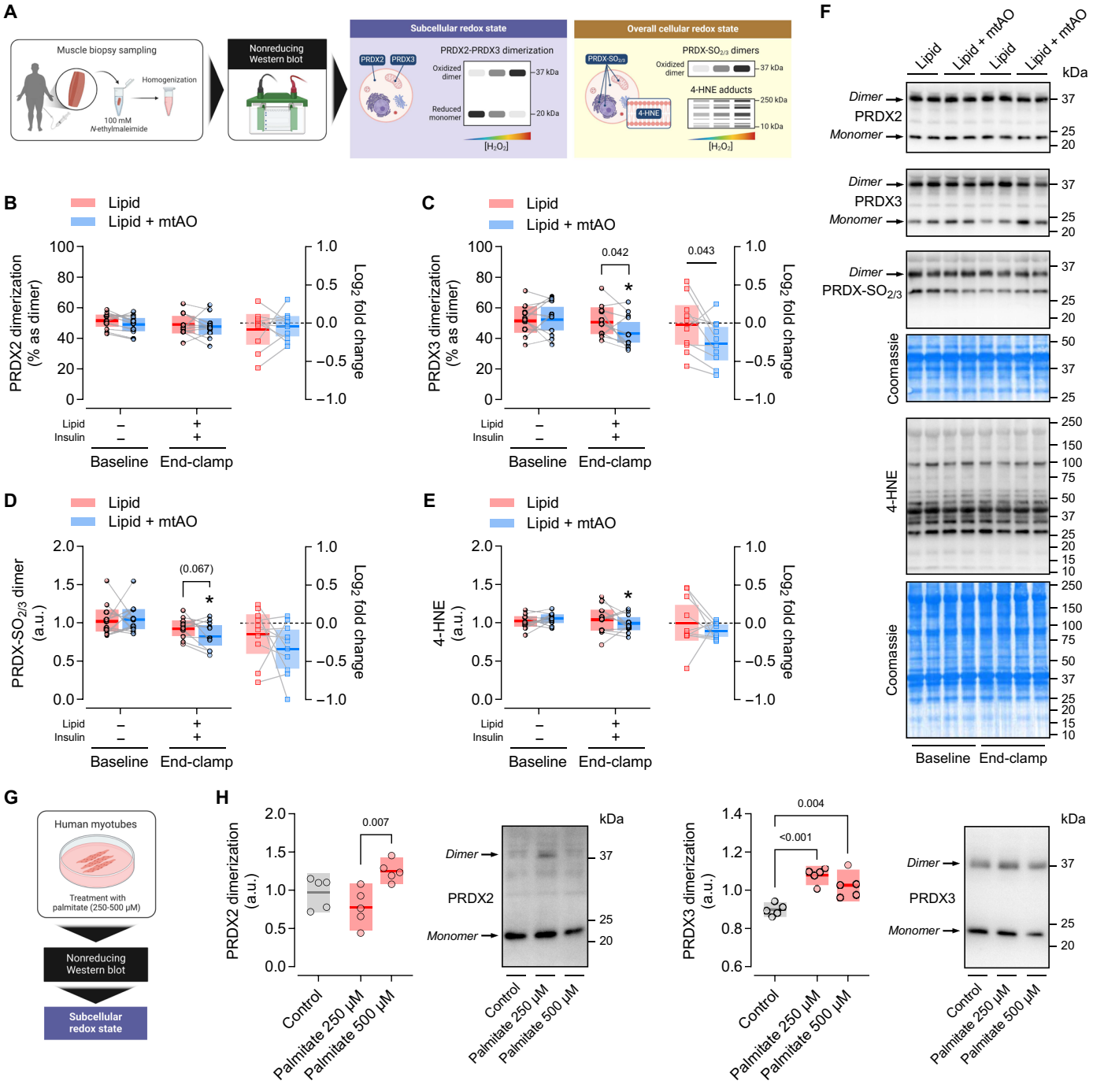

Fig. 5. The mtAO mitoquinone reduces the muscle mitochondrial oxidative burden under lipid overload. (**A**) Workflow to quantitatively analyze redox-sensitive proteins and lipid peroxidation in skeletal muscle biopsy samples. (**B**) Cytosolic oxidative burden as determined by protein abundance of peroxiredoxin 2 (PRDX2) dimers relative to monomers in whole-muscle homogenates. (**C**) Mitochondrial oxidative burden as determined by protein abundance of peroxiredoxin 3 (PRDX3) dimers relative to monomers in whole-muscle homogenates. (**D**) Overall peroxiredoxin oxidation as determined by protein abundance of oxidized/hyperoxidized peroxiredoxin (PRDX-$SO_{2/3}$) dimers in whole-muscle homogenates. (**E**) Whole-muscle lipid peroxidation as determined by protein abundance of 4-hydroxynonenal (4-HNE) adducts in whole-muscle homogenates. (**F**) Representative blots related to the experiments in human skeletal muscle biopsy samples ($n = 2$ biological replicates from each muscle biopsy sample for each patient). Coomassie blue staining was used as a loading control for PRDX-$SO_{2/3}$ and 4-HNE. (**G** and **H**) Cytosolic and mitochondrial oxidative burden in human myotubes treated with either vehicle BSA (control; $n = 5$), 250 µM palmitate ($n = 5$), or 500 µM palmitate. Relative PRDX2 and PRDX3 dimer abundance (dimer-to-monomer ratio) was normalized to cell plate–specific mean dimerization to adjust for *N*-ethylmaleimide treatment efficiency. Human data are presented as observed individual values with estimated means ±95% confidence limits. Linear mixed models were used to estimate within- and between-treatment differences (B to E). *Different from Baseline ($P < 0.05$). $n = 10$ for all measurements. Human muscle cell data are presented as observed values with means ±95% confidence limits. A one-way ANOVA was used to estimate between-treatment differences (H). Illustrations in (A) and (G) were created with BioRender.com.

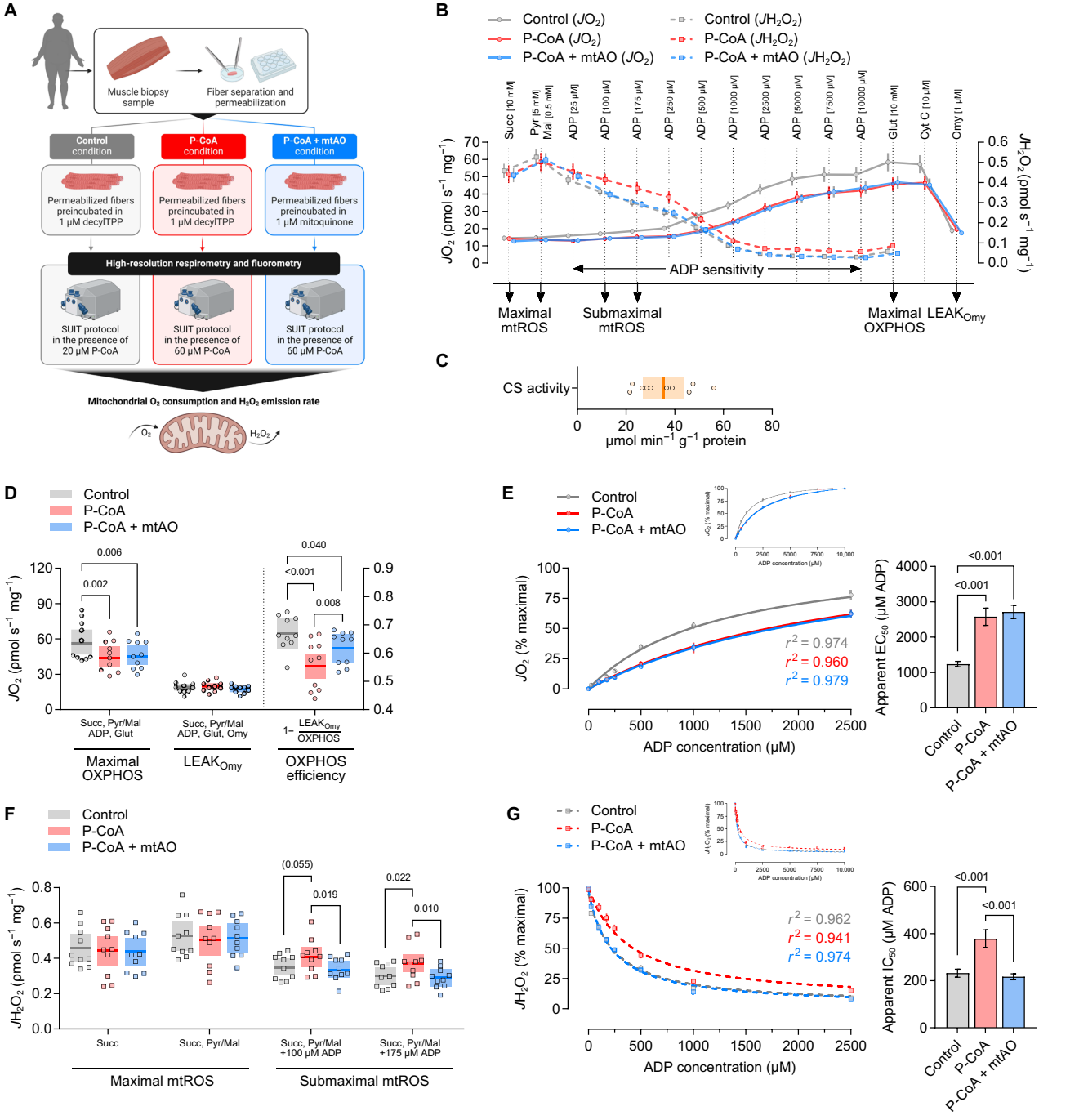

Fig. 6. The mtAO mitoquinone improves muscle mitochondrial bioenergetics under lipotoxic conditions. (**A**) Workflow to determine ex vivo mitochondrial bioenergetics in human skeletal muscle, i.e., in permeabilized fiber bundles (PmFBs), using a substrate-inhibitor titration (SUIT) protocol reflecting normal (20 µM P-CoA) versus high (60 µM P-CoA) intramyocellular lipid conditions. PmFBs were preincubated in either decylTPP (control compound) or mitoquinone to evaluate the effects of mtAO on lipid-induced mitochondrial stress. (**B**) SUIT protocol used to simultaneously measure mitochondrial O_2 consumption (JO_2) and H_2O_2 emission (JH_2O_2) rates. Succinate (Succ); pyruvate (Pyr); malate (Mal); adenosine diphosphate (ADP); glutamate (Glut); cytochrome C (Cyt C); oligomycin (Omy). Data are means ± SEM. (**C**) Muscle mitochondrial content, as determined by citrate synthase (CS) activity in muscle homogenates obtained from separate portions of the biopsy specimen used for assessments of mitochondrial bioenergetics. Data are presented as individual values with estimated mean ± 95% confidence limits. (**D**) Maximal mitochondrial oxidative phosphorylation capacity (OXPHOS), oligomycin-induced leak respiration ($LEAK_{Omy}$), and OXPHOS efficiency [calculated as 1 − RCR = 1 − $LEAK_{Omy}$/OXPHOS (*100*)]. Data are presented as individual values with estimated means ±95% confidence limits. (**E**) Sensitivity of mitochondrial JO_2 to ADP. The apparent half-maximal effective concentration (EC_{50}) for ADP was determined using [agonist] versus response (three parameters) analysis in GraphPad Prism. Data are means ± SEM. (**F**) Maximal and submaximal mitochondrial H_2O_2 emission rates. Data are presented as individual values with estimated means ±95% confidence limits. (**G**) Sensitivity of mitochondrial JH_2O_2 to ADP. The apparent half-maximal inhibitory concentration (IC_{50}) for ADP was determined using [inhibitor] versus response (three parameters) analysis in GraphPad Prism. Data are means ± SEM. A linear mixed model [(D) and (F)] or one-way ANOVA [(E) and (G)] was used to estimate between-treatment differences. $n = 10$ for all measurements. Illustrations in (A) were created with BioRender.com.

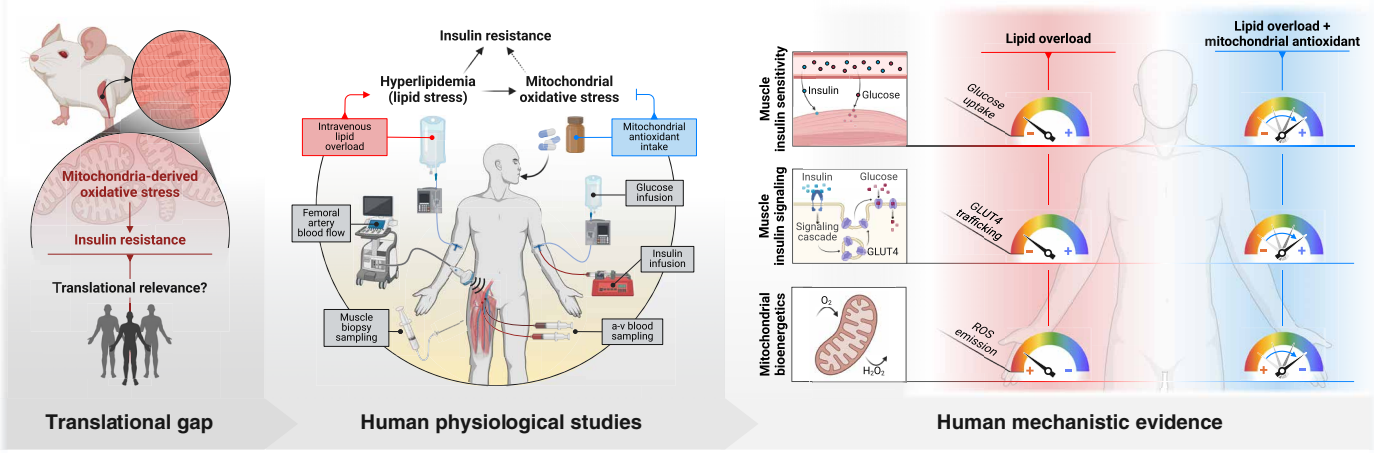

Fig. 7. Experimental framework of the study. Conceptual and experimental framework providing mechanistic evidence that mitochondrial redox state influences muscle insulin action in humans. Illustration created with BioRender.com.

hyperinsulinemic clamp conditions, muscle insulin resistance is often accompanied by decreased rates of whole-body glucose disposal (*3*). Our data indicate that the robust effect of the mtAO mitoquinone on muscle insulin sensitivity was nonsignificant at the whole-body level, implying divergent effects in skeletal muscle and liver insulin sensitivity. Although an explanation for this is not apparent, a potential mechanism might involve redox-dependent regulation of Angiopoietin-like protein 4 (ANGPTL4), an endocrine factor that inhibits lipoprotein lipase (*88*) and promotes the accumulation of hepatic triglycerides in HFD-fed mice (*89*, *90*). Given that treatment with the antioxidant Tempol upregulates ANGPTL4 in mice under HFD feeding conditions (*91*), it is tempting to speculate a similar effect of mitoquinone in the present lipid overload model, resulting in a greater fatty acid flux to the liver, which ultimately exacerbated the impairments in insulin-mediated suppression of hepatic glucose production.

Lipid oversupply may impair muscle insulin sensitivity via a multitude of mitochondria-dependent mechanisms, including (i) mitochondrial substrate competition (*56*, *92*), (ii) mitochondrial dysfunction–driven accumulation of intramuscular lipids (*5*), and (iii) excessive mitochondrial fatty acid oxidation (*7*). Here, intake of the mtAO mitoquinone was not associated with alterations in either leg substrate oxidation or leg lactate release, suggesting a marginal role of mitochondrial substrate competition in the observed mitigation of lipid-induced muscle insulin resistance. Regarding intramuscular lipid accumulation, there is contrasting evidence for this phenomenon to occur upon acute lipid overload. One study observed an increase in muscle ceramides (*93*) as opposed to a number of studies showing no changes upon Intralipid infusion (*43*, *52*, *55*, *94*). Likewise, an Intralipid-induced increase in muscle diacylglycerol levels has been reported in some (*52*, *55*), but not all (*43*), human studies. Intramuscular lipid accumulation has been proposed as a prominent cause of muscle insulin resistance in light of data showing that intramuscular lipids inhibit insulin signaling (*52*–*54*). Such intramuscular lipid accumulation may occur via release of lipid intermediates from the mitochondria to the cytosol as a result of increased mitochondrial fission/fragmentation upon Intralipid infusion (*95*). Because we did not observe mitoquinone-mediated alterations in insulin signaling, it is likely that, if intramuscular lipid accumulation occurred in the present study, mechanisms other than rescued insulin signaling contributed to alleviating insulin resistance. In this direction, myocellular accumulation of lipid intermediates may inhibit mitochondrial ADP transport, ultimately increasing mitochondrial membrane potential and ROS production (*24*, *25*); thus, it is plausible that mitoquinone attenuated the rise in mitochondrial oxidative burden associated with increased intramuscular lipid availability. Similarly, it is also likely that mitoquinone mitigated mitochondrial oxidative stress arising from the elevated β-oxidation associated with lipid oversupply.

Our finding that mitoquinone-dependent improvements in muscle insulin sensitivity occurred irrespective of enhancements in canonical insulin signaling, but in association with increased GLUT4 translocation, is in line with data showing that selective induction of mtROS in muscle cells impairs insulin-stimulated GLUT4 translocation but not insulin signaling to Akt or Akt substrates (*35*). Notably, the relatively small increase, or lack of change, in sarcolemmal GLUT4 observed upon insulin stimulation contrasts with the marked increase in muscle glucose uptake detected in either the presence or absence of mitoquinone; this was possibly due to the combination of two factors. First, the subcellular fractionation approach may underestimate GLUT4 translocation; indeed, despite a 100-fold increase in muscle glucose uptake, only a 2-fold increase in plasma membrane GLUT4 has been reported in response to exercise (*96*). Second, the prediabetic state of our study participants might have further blunted the responsiveness of GLUT4 to insulin stimulation; in fact, increments in plasma membrane GLUT4 during a hyperinsulinemic clamp have been shown to be apparent in healthy individuals but not in patients with type 2 diabetes (*60*). The present human results were substantiated by complementary experiments in (i) rodent muscle cells, where mitoquinone rescued lipid-induced impairments in GLUT4 translocation, and (ii) rodent muscle fibers, where selective induction of mitochondrial oxidative stress impaired insulin-mediated GLUT4 translocation. Altogether, our findings indicate that a pro-oxidative shift in mitochondrial redox state is necessary and sufficient to disrupt GLUT4 translocation in skeletal muscle.

Here, the mitochondria-targeted CoQ derivative mitoquinone was used as a tool to selectively target mitochondrial redox state. Mitoquinone is a ubiquinone moiety linked to a lipophilic cation, which enables it to pass through the plasma membrane and then accumulate into mitochondria driven by the plasma and the mitochondrial

membrane potential, respectively (*32*). Inside the mitochondrion, mitoquinone is absorbed to the mitochondrial inner membrane, where it acts as an antioxidant, primarily by preventing lipid peroxidation (*32*). The mitoquinone-mediated protection of mitochondrial lipids from oxidative damage may indirectly reduce mtROS production. The mitochondrial inner membrane is rich in phospholipids very susceptible to ROS-induced peroxidation (*97*), which may compromise the mitochondrial membrane structure and function, ultimately generating a chain reaction that induces a further increase in mtROS (*98*). In this scenario, mitoquinone may act as a chain-breaking antioxidant. Herein, through assessments of muscle subcellular redox state, we observed that mitoquinone reduced the mitochondrial oxidative burden, as measured by PRDX3 dimerization, without affecting the cytosolic redox state or the degree of lipid peroxidation when compared with placebo. While the lack of substantial effects on lipid peroxidation should be interpreted with caution (4-HNE adducts were quantified in whole muscle homogenates, possibly lacking the sensitivity to detect the mitochondria-specific alterations elicited by mitoquinone), the present data demonstrate a mitochondria-specific antioxidant action of mitoquinone in human muscle under lipid stress, a finding that contrasts with a study reporting no effect of long-term mitoquinone treatment on age-related redox stress in rodent skeletal muscle (*99*) and that possibly underlines the treatment duration–dependent effects of mitoquinone on muscle redox state.

The mitochondria-specific antioxidant effect of mitoquinone in human muscle was confirmed by assessments of mitochondrial bioenergetics ex vivo, where it prevented lipid-induced increments in mitochondrial H_2O_2 emission. These findings are consistent with the potential of mtAO to rescue impairments in muscle mitochondrial bioenergetics (*75*). Notably, these effects were apparent only in the presence of substrates resembling the resting skeletal muscle metabolic milieu, thus pertaining to submaximal mtROS production. Succinate-mediated maximal mitochondrial H_2O_2 emission rates were unaffected by either mitoquinone or lipid stress, which contrasts with preclinical data showing that treatment with the mtAO SS-31 reversed the increase in maximal mitochondrial H_2O_2 emission caused by a short-term HFD (*28*).

Overall, these outcomes not only underscore the importance of assessing mitochondrial bioenergetic function under biologically relevant conditions in human muscle (*100*, *101*) but also suggest that lipid-induced muscle mitochondrial stress is unlikely to be driven by H_2O_2 originating from complex I via succinate-induced reverse electron transport (RET). This aligns with in vitro studies showing that fatty acids increase mtROS generation under conditions of forward rather than reverse electron transport (*102*). Similarly, our ex vivo muscle experiments did not show apparent effects of mitoquinone on succinate-mediated mtROS production, as otherwise reported in rat heart mitochondria (*103*). On the other hand, succinate-mediated mtROS production was determined under saturating concentrations of succinate; thus, it cannot be ruled out that lipid stress– or mitoquinone-dependent alterations would have been apparent in the presence of nonsaturating succinate levels. Likewise, the lack of effect of mitoquinone on succinate-mediated mtROS production may be due to a relatively small magnitude of effect of mitoquinone under experimental conditions that stimulate maximal mtROS production.

Considering that, in muscle cells under resting conditions, RET (i.e., site I_Q) and the outer quinone-binding site at complex III (site III_{Q0}) are the main mitochondrial sources of total cellular H_2O_2 release, and together contribute to the vast majority of $O_2^{\cdot-}/H_2O_2$ release in the mitochondrial matrix (*104*), it is tempting to speculate that site III_{Q0} was the predominant mitochondrial source of ROS under lipid stress and that mitoquinone, by influencing the redox state of the CoQ pool, indirectly attenuated lipid-induced H_2O_2 release from site III_{Q0}. In this direction, the application of novel pharmacological tools, such as S1QEL and S3QEL molecules suppressing mtROS production at specific sites of the electron transport chain (*105*), will allow to interrogate the role of given mtROS sources in the pathophysiology of muscle insulin resistance.

Limitations and perspectives

The present study has some limitations. Owing to the invasiveness of the clinical procedures, the sample size of this proof-of-concept study was relatively small and restricted to a homogeneous cohort of adult males with prediabetes. The present participants were chosen for being insulin resistant but not yet treated with glucose- or lipid-lowering medications, which may affect muscle mitochondrial biology (*106*, *107*). Females were not included to avoid confounding effects of menstrual cycle–dependent fluctuations in hormones influencing insulin action (*108*). Future studies should explore whether the mechanistic link between mitochondrial redox state and muscle insulin sensitivity is influenced by sex, age, and metabolic health status.

This study was designed to interrogate a putative mechanism underlying muscle-specific insulin resistance. While comprehensive assessments were conducted at the skeletal muscle level, neither hepatic insulin sensitivity nor hepatic glucose metabolism was evaluated. Hence, it remains unclear whether selective targeting of mitochondrial redox state differentially affects muscle and liver insulin action. To interrogate the muscle tissue–specific delivery of orally administered mitoquinone, and thus infer its muscle-specific action, we conducted preliminary studies demonstrating that mitoquinone is taken up by skeletal muscle after administration of a single oral dose (fig. S2). However, given the cell type–specific effects of mitoquinone (*109*), further studies are required to elucidate tissue-specific pharmacodynamic properties of mitoquinone in humans. In addition, although mitoquinone is a mitochondria-targeted CoQ derivative, it appears to reduce mtROS generation without significant changes in the CoQ redox state (*103*). Therefore, it is yet to be determined whether the antioxidant effect of mitoquinone in human skeletal muscle mitochondria is causally driven by upstream modifications in the CoQ pool. If this is the case, the reported insulin-sensitizing effects of mitoquinone would align with emerging evidence linking CoQ deficiency to peripheral insulin resistance (*23*, *110*).

The present ex vivo assessments of muscle mitochondrial bioenergetics provide insights into how mitoquinone protects against lipid-induced mitochondrial malfunction. However, these experiments modeled mitochondrial stress elicited by cytosolic lipid accumulation. Further investigation is required to elucidate whether mitoquinone, and mtAO more broadly, can improve mitochondrial bioenergetics under conditions modeling excessive fat oxidation. Moreover, these experiments did not fully replicate the muscle metabolic milieu characterizing the hyperinsulinemic-hyperlipidemic state of the in vivo human experiments. Therefore, the protective effects of mitoquinone in muscle ex vivo do not necessarily explain the insulin-sensitizing effects observed in vivo.

Clinical implications

In conclusion, this proof-of-concept physiological study delineates a conserved role of mitochondria-derived ROS in the development

of lipid-induced insulin resistance in human skeletal muscle, thus bridging the translational gap from preclinical models. Altogether, our findings provide mechanistic insights into how mitochondrial biology affects muscle insulin action in humans and corroborate preclinical data proposing that mitochondrial oxidative stress causes insulin resistance by impairing insulin-stimulated GLUT4 translocation.

It is worth noting that muscle insulin resistance is multifactorial and may arise also from a lack of contractile activity. In this context, prolonged bed rest markedly reduces insulin sensitivity in the absence of concurrent alterations in muscle mtROS production (*111*), implying that alterations in mitochondrial redox state might be of secondary importance in inactivity- versus overnutrition-induced insulin resistance. From a clinical standpoint, the present findings underscore the therapeutic potential of mitochondrial redox targeting against obesity-related insulin resistance, thus providing an incentive for larger-scale trials addressing the clinical significance of mitochondria-targeted therapy in the context of metabolic diseases.

MATERIALS AND METHODS

Human studies

Study design

The objective of this proof-of-concept mechanistic study was to interrogate the role of mitochondrial oxidative stress in human skeletal muscle insulin resistance. To this end, we conducted insulin clamp studies combining intravenous infusion of a lipid overload with intake of mtAO in a single-blinded randomized placebo-controlled crossover fashion. The study was approved by the Regional Ethics Committee of Copenhagen, Denmark (H-19031551) and adheres to the principles of the Declaration of Helsinki. This study was part of a larger clinical trial investigating distinct mechanisms influencing insulin sensitivity. The overall trial protocol was registered at ClinicalTrials.gov (identifier: NCT04558190).

Because no prior clinical data were available on the effects of mtAO on muscle insulin sensitivity, sample size was determined based on a preclinical study achieving a power of 0.82 (effect size $d = 1.55$; $\alpha = 0.05$) when comparing a surrogate measure of insulin sensitivity [homeostatic model assessment of insulin resistance (HOMA-IR)] between two independent groups of eight rodents fed an HFD versus HFD combined with mtAO (*34*). Given the greater specificity, accuracy, and sensitivity of the hyperinsulinemic clamp technique, we assumed a larger treatment effect size of mtAO on clamp-based measures of insulin sensitivity as compared with surrogate measures of insulin sensitivity. Accordingly, a sample size of 10 participants in a crossover design was deemed to be large enough to achieve a power ≥ 0.80.

Twelve adult males with overweight and prediabetes enrolled in the study. Participants were informed of risks and discomfort associated with the experimental procedures and provided written informed consent before inclusion in the study. One participant withdrew from the study before the experimental trials due to major illness, whereas one participant was excluded during the first experimental trial due to anatomical incompatibility with the femoral catheters. Therefore, data from 10 participants who completed the study are reported here (fig. S1). Inclusion criteria were as follows: (i) male, (ii) age 40 to 60 years old, (iii) body mass index 25 to 40 kg/m^2, (iv) fasting plasma glucose ≥5.6 mM or HbA1c ≥5.7%, (v) HOMA2-IR >1.4, and (vi) sedentary lifestyle [<3 hours of physical activity/week and maximal oxygen uptake ($\dot{V}_{O2max}$) <45 ml kg^{-1} min^{-1}]. Exclusion criteria were as follows: (i) current treatment with antidiabetic medications or insulin; (ii) diagnosed thyroid, liver, heart, or kidney disease; (iii) use of medications known to affect study outcome measures or increase the risk of study procedures; (iv) use of mitoquinone or dietary supplements containing CoQ-10 within 30 days before the screening appointment; (v) smoking or use of tobacco products; (vi) recent weight gain or loss (>5% change within 2 months before inclusion in the study); and (vii) excessive alcohol consumption (alanine aminotransferase >55 U/liter). Participant characteristics are presented in Table 1.

Screening visits

Potential participants underwent a prescreening telephone interview followed by two in-person screening visits to assess eligibility criteria. The first screening visit comprised a complete medical history and a physical examination including lung and heart auscultation, electrocardiogram, blood pressure monitoring, and a fasting blood test. The second screening visit comprised assessments of body composition and cardiorespiratory fitness. Body composition parameters were determined using dual-energy x-ray absorptiometry (Lunar iDXA; GE Healthcare, GE Medical Systems, Belgium) after at least 4 hours of fasting. Cardiorespiratory fitness ($\dot{V}_{O2max}$) was determined during an incremental test to exhaustion on a mechanically braked cycle ergometer (LC7; Monark Exercise AB, Vansbro, Sweden). The test protocol included a 4-min bout at 80 W followed by an incremental test with increments of 20 W/min until volitional exhaustion. Pulmonary gas exchanges were measured breath-by-breath using an online gas analysis system (Oxycon Pro, Viasys Healthcare, Hoechberg, Germany).

Experimental trials

Participants attended two experimental trials on separate occasions interspersed by 14 days. The experimental trials consisted of (i) a hyperinsulinemic-isoglycemic clamp combined with intravenous infusion of a lipid emulsion and oral administration of placebo ("Lipid" trial), and (ii) a hyperinsulinemic-isoglycemic clamp combined with intravenous infusion of a lipid emulsion and oral administration of mtAO ("Lipid + mtAO" trial).

Participants were instructed to maintain their usual lifestyle during the study period, i.e., individual interviews were conducted before each experimental trial day to ensure that no changes in dietary habits and physical activity routine occurred. Before the first experimental trial day, participants recorded food intake for 3 days, which was replicated before the second experimental trial day. Participants abstained from caffeine, alcohol, and exercise for 48 hours before the experimental trial days.

Administration of mtAO

Preliminary studies were conducted in a cohort of healthy young males ($n = 6$; age 24.5 ± 3.6 years, height 185 ± 10 cm, weight 87.5 ± 12.5, and $\dot{V}_{O2max}$ 52.6 ± 4.7 ml kg^{-1} min^{-1}) to determine pharmacokinetic parameters of the mtAO mitoquinone in skeletal muscle after administration of a single oral dose (ClinicalTrials.gov identifier: NCT04098510). Exclusion criteria were previous use of mitoquinone or CoQ-10 within 30 days of the screening appointment, ongoing treatment with medications, and smoking. Participants attended an experimental trial in the morning after an overnight fast and were instructed to abstain from caffeine, alcohol, and exercise for 24 hours before the appointment. After 10 min of supine rest, a 3-mm incision was made over the lateral portion of the thigh under local anesthesia and a biopsy (Pre-dose) was obtained from the vastus lateralis muscle using a percutaneous Bergstrom needle with suction. Thereafter, participants ingested a single oral dose of mitoquinone (160 mg), corresponding to the

maximal dose documented to elicit acute physiological effects in humans in vivo without incurring serious adverse events (*47*). Participants remained in the laboratory lying on a bed and were allowed to consume only water ad libitum. Additional biopsies were obtained from the vastus lateralis muscle at 1, 3, and 5 hours after administration of mitoquinone (fig. S2A). Upon collection, muscle biopsy samples were washed in ice-cold saline to reduce blood contamination, dried, frozen in liquid N_2, and stored in cryotubes at −80°C until analysis. Mitoquinone content in skeletal muscle was quantified by liquid chromatography–tandem mass spectrometry, as previously described (*112*). None of the participants reported adverse events following mitoquinone administration.

The average maximum measured muscle concentration of mitoquinone (C_{max}; 3.84 ± 1.10 pmol/g) was observed 3 hours after administration (fig. S2B). These data demonstrate that mitoquinone is taken up by human skeletal muscle in vivo, aligning with prior data showing mitoquinone levels of ~20 pmol/g in mouse muscle following long-term treatment with 500 μM mitoquinone (*112*). It should be noted that the relatively low levels detected in humans as compared with mouse muscle are likely due to the prolonged treatment and the markedly higher dose administered in mice, i.e., ~80 mg/kg, which corresponds to a human equivalent dose of 6.6 mg/kg (*113*) as compared with the 1.6 mg/kg dose administered in our study. In light of this preliminary data, the main study included a short-term treatment period with escalating doses of mitoquinone to maximize muscle tissue accumulation and reduce any potential gastrointestinal discomfort associated with the high dose administered on the experimental trial day. Specifically, participants ingested daily doses of 40, 80, and 120 mg mitoquinone (or placebo) within the 3 days before the experimental trial day (fig. S2C). On the experimental trial day, a dose of 80 mg was administered 3 and 1 hour before the initiation of the hyperinsulinemic-isoglycemic clamp to achieve and maintain maximum muscle concentration of mitoquinone throughout the 120-min clamp period.

Hyperinsulinemic-isoglycemic clamp

Participants reported to the laboratory in the morning after an overnight fast (~10 hours). Arrow catheters (20 gauge; Teleflex, Wayne, PA, USA) were inserted into the femoral artery and vein of the right leg under local anesthesia (2 ml of lidocaine without epinephrine, 20 mg/ml Xylocaine) to obtain arterial and venous blood samples. Catheters were placed ~3 cm below the inguinal ligament and advanced 10 cm in the proximal direction. Correct catheter placement was verified using ultrasound Doppler (Vivid E9; GE Healthcare, Waukesha, WI, USA). In addition, catheters were inserted into the antecubital veins for infusions. Thereafter, intravenous infusion of heparinized [0.2 U min^{-1} kg^{-1} body mass (BM)] lipid emulsion (1.15 ml $hour^{-1}$ kg^{-1} BM; Fresenius-Kabi, Intralipid 20% 500 ml) was initiated, and the first dose of mitoquinone (80 mg) or placebo was administered. After 2 hours of lipid infusion, the second dose of mitoquinone (80 mg) or placebo was administered. After 3 hours of lipid infusion, a hyperinsulinemic-isoglycemic clamp was initiated with a bolus of insulin (9.0 mU/kg BM; Novo Nordisk, Actrapid 10 ml) followed by 120 min of constant insulin infusion (1.42 mU min^{-1} kg^{-1} BM). During the clamp, glucose was infused from a 20% glucose solution (Fresenius-Kabi). Arterial plasma glucose was measured every 7.5 min, and the glucose infusion rate was adjusted to match isoglycemia, defined as the overnight-fasting arterial glucose concentration measured at baseline on the first experimental trial day. Femoral artery blood flow was measured, and blood was collected simultaneously from the femoral artery and femoral vein at −180, 0, 30, 60, 90, 105, and 120 min of the clamp (Fig. 1B).

Femoral artery blood flow

Femoral artery blood flow was determined by ultrasound Doppler (Vivid E9; GE Healthcare) equipped with a linear probe operating at an imaging frequency of 8.0 MHz and Doppler frequency of 3.1 MHz. Measurements were conducted in triplicate, i.e., three consecutive 15-s recordings were acquired at each time point, and the average value from the three replicate measurements was calculated.

Blood and plasma analyses

Femoral arterial and venous blood samples were drawn in heparinized 2-ml syringes for immediate analysis of glucose, lactate, hematocrit, partial pressure of O_2 (PO_2) and CO_2 (PCO_2), O_2 saturation, hemoglobin concentration, pH, and bicarbonate ions using an ABL800 Flex (Radiometer, Copenhagen, Denmark).

In addition, before the lipid infusion as well as before and after the hyperinsulinemic-isoglycemic clamp, an arterial blood sample was collected in 5-ml syringes and transferred to an Eppendorf tube containing 30 μl of EDTA (0.2 M), after which it was centrifuged at 20,000*g* for 3 min to collect plasma, which was stored at −80°C until analysis for plasma insulin, free fatty acids, and catecholamines. Plasma insulin concentration was measured using an enzyme-linked immunosorbent assay (ELISA) kit (ALPCO, 80-INSHU-E01.1). Plasma free fatty acid concentration was measured using an enzymatic colorimetric assay (Wako Chemicals) adapted for the Pentra C400 (Horiba Medical). The kit reagents were reconstituted according to the manufacturer's instructions, and the method was calibrated with a standard solution of oleic acid (1.0 mM) contained in the kit. Plasma adrenaline and noradrenaline concentrations were determined by using an ELISA kit (LDN, BA E-4500). All the blood and plasma analyses were conducted in technical duplicates.

Leg muscle mass

The total muscle mass of the experimental leg was calculated as 83% of the leg lean mass, as measured by dual-energy x-ray absorptiometry (Lunar iDXA, GE Healthcare, GE Medical Systems, Belgium) (*114*). The leg region, defined as the area extending from the inferior border of the ischial tuberosity to the distal tip of the toes, was adjusted using enCORE Forma v.15 software (GE Healthcare Lunar, Buckinghamshire, UK).

Calculations

Muscle glucose uptake and muscle lactate release, as measured by the net exchange of substrates (glucose and lactate) across the leg muscles, were calculated from the femoral arterial plasma flow (F_p, expressed per kilogram of leg muscle mass) and the arteriovenous difference in plasma concentration of the given substrate ($substrate_{a\text{-}v}$), which was corrected for changes in plasma volume by accounting for the net transcapillary water flux (J_v) (*115*, *116*)

$$\text{Net Exchange}_{\text{substrate}} = F_p \times \text{substrate}_a - \left(F_p - J_v\right) \times \text{substrate}_v$$

The femoral arterial plasma flow (F_p) was calculated as

$$F_p = F \times \left(1 - \frac{\text{Hct}_a}{100}\right)$$

where F is the femoral arterial blood flow and Hct_a is the arterial hematocrit.

The net transcapillary water flux (J_v) into or out of the vein was calculated as

$$J_v = F \times \left\{ \left[\left(\frac{Hb_a}{Hb_v} \right) \times \left(\frac{100 - Hct_v}{100 - Hct_a} \right) \right] - 1 \right\}$$

where Hb_a and Hb_v are the arterial and venous hemoglobin concentration, respectively, and Hct_v is the venous hematocrit.

Leg O_2 consumption ($\dot{V}O_2$), leg CO_2 release ($\dot{V}_{CO2}$), and leg respiratory quotient (RQ) were calculated from the femoral artery blood flow (F) and the arteriovenous difference in content of the given gas

$$\dot{V}_{O_2} = F \times \left(Ca_{O_2} - Cv_{O_2} \right)$$

$$\dot{V}_{CO_2} = F \times \left(Ca_{CO_2} - Cv_{CO_2} \right)$$

$$RQ = \frac{\dot{V}_{CO_2}}{\dot{V}_{O_2}}$$

Content of O_2 and CO_2 in arterial blood (Ca_{O2} and Ca_{CO2}) and venous blood (Cv_{O2} and Cv_{CO2}) was computed using the equations by Siggaard-Andersen *et al.* (*117*). Glucose and lipid oxidation across the leg were estimated from the leg $\dot{V}O_2$ and $\dot{V}CO_2$ using the equations by Péronnet and Massicotte (*118*).

Muscle biopsies

Muscle biopsies were obtained from the vastus lateralis muscle before lipid infusion (Baseline), as well as immediately before (Pre-clamp) and after (End-clamp) the hyperinsulinemic-isoglycemic clamp (Fig. 1B). Biopsies were taken through separate incisions made over the lateral portion of the experimental thigh under local anesthesia [1 ml of lidocaine without epinephrine, Xylocaine (20 mg/ml), AstraZeneca] using a percutaneous Bergström needle with suction.

Upon collection, muscle biopsy samples were washed with ice-cold saline to reduce blood contamination. The sampled biopsies were then divided into different portions, which were handled differently according to subsequent analyses. Specifically, a portion was snap frozen in liquid N_2 and stored at −80°C for subsequent immunoblotting and enzymatic activity analyses. Another portion was quickly immersed in phosphate-buffered saline (PBS) containing 100 mM *N*-ethylmaleimide (NEM; a fast-acting membrane permeable alkylating agent) for 5 min, snap frozen in liquid N_2, and stored at −80°C for subsequent nonreducing SDS–polyacrylamide gel electrophoresis (SDS-PAGE) and Western blotting. A fraction (~20 mg wet weight) of the biopsy specimen sampled at Baseline on the Lipid trial day was immediately placed in ice-cold biopsy preservation solution and prepared for assessments of mitochondrial bioenergetics.

Immunoblotting

Protein abundance in whole-muscle homogenate lysates or plasma membrane fractions was determined by SDS-PAGE and Western blotting. Protein markers of muscle redox state (peroxiredoxin dimerization and 4-HNE) were resolved by SDS-PAGE under nonreducing conditions (*119*).

Whole-muscle homogenate lysate preparation, SDS-PAGE, and Western blotting. Muscle samples were freeze dried for 48 hours and dissected free of blood, fat, and connective tissue. Dissection was performed under a stereo microscope with ambient temperature of ~18°C and relative humidity <30%. After dissection, muscle tissue was weighed, and a fresh batch of ice-cold homogenization buffer [10% glycerol, 20 mM Na-pyrophosphate, 150 mM NaCl, 50 mM Hepes (pH 7.5), 1% Nonidet P-40 (NP-40), 20 mM β-glycerophosphate, 2 mM Na_3VO_4, 10 mM NaF, 2 mM PMSF, 1 mM EDTA (pH 8), 1 mM EGTA (pH 8), aprotinin (10 μg/ml), leupeptin (10 μg/ml), and 3 mM benzamidine] was added to the tube containing the freeze-dried tissue. NEM (100 mM) was included in the homogenization buffer used for the samples undergoing nonreducing SDS-PAGE. Freeze-dried muscle samples (≈2 mg dry weight) were homogenized 2 × 2 min at 28.5 Hz in a TissueLyser (Qiagen TissueLyser II, Retsch GmbH, Haan, Germany Qiagen). Afterward, the samples were rotated for 1 hour at 4°C and sonicated (Branson Digital Sonifier) 2 × 10 s at 10% amplitude. The total protein concentration in each homogenate lysate sample was determined using a bovine serum albumin (BSA) standard kit (Thermo Fisher Scientific; assayed in triplicate). Each homogenate lysate sample was then mixed with 6 × Laemmli buffer (7 ml of 0.5 M tris base, 3 ml of glycerol, 0.93 g of DTT, 1 g of SDS, and 1.2 mg of bromophenol blue) and double-distilled H_2O to reach equal protein concentration (2.0 μg/μl). DTT was not included in the buffer used for the samples subjected to nonreducing SDS-PAGE.

Equal amounts of total protein were loaded for each sample in precast gels (Criterion TGX Stain-Free Precast Gels, Bio-Rad, Copenhagen, Denmark). All the samples from each individual participant were loaded onto the same gel. Individual gels were compared using the same internal gel standard sample. Proteins were separated according to their molecular weight by SDS-PAGE and semi-dry transferred to a polyvinylidene difluoride (PVDF) membrane (Millipore, Denmark). The membranes were blocked in either 2% skim milk or 3% BSA in tris-buffered saline-Tween 20 (TBST) before being incubated overnight at 4°C in primary antibody diluted in either 2% skim milk or 3% BSA. After washing in TBST, the membranes were incubated with a secondary horseradish peroxidase–conjugated antibody for 1 hour at room temperature. The secondary antibodies were diluted 1:5000 in 2% skim milk or 3% BSA depending on the primary antibody. Membrane staining was visualized by incubation with a chemiluminescent horseradish peroxidase substrate (Immobilon Forte, Millipore, Denmark) before image digitalization on ChemiDoc MP (Bio-Rad). Western blot band intensity was determined by densitometry quantification (total band intensity adjusted for background intensity) using Image Lab Software v.6.0 (Bio-Rad Laboratories). For insulin signaling proteins, phosphorylated and total protein content were determined on separate membranes in separate analyses, and none of the membranes were stripped before protein quantification. Analyses were performed in duplicate for each biological sample; i.e., two separate samples were obtained from the same muscle specimen upon dissection, and the average signal intensity from the two samples was used as the result.

Plasma membrane fraction preparation, SDS-PAGE and Western blotting. Plasma membrane proteins were isolated from frozen muscle samples (~15 mg wet weight) using the Minute Plasma Membrane Protein Isolation Kit (Invent Biotechnologies Inc., SM-005) according to the manufacturer's instructions. The pellet containing plasma membrane proteins was dissolved in 30 μl of a fresh batch of ice-cold homogenization buffer [10% glycerol, 20 mM Na-pyrophosphate, 150 mM NaCl, 50 mM Hepes (pH 7.5), 1% NP-40, 20 mM β-glycerophosphate, 2 mM Na_3VO_4, 10 mM NaF, 2 mM PMSF, 1 mM EDTA (pH 8), 1 mM EGTA (pH 8), aprotinin (10 μg/ml), leupeptin (10 μg/ml), and 3 mM benzamidine]. Each homogenate lysate sample was then mixed with 6 × Laemmli buffer (7 ml of 0.5 M

tris base, 3 ml of glycerol, 0.93 g of DTT, 1 g of SDS, and 1.2 mg of bromophenol blue) and double-distilled H_2O.

Equal volumes (10 μl) of plasma membrane homogenate lysates were loaded for each sample in precast gels (7.5% Criterion TGX Stain-Free Precast Gels, Bio-Rad). The samples from each individual participant were loaded onto the same gel. Individual gels were compared using the same internal gel standard sample. Proteins were separated according to their molecular weight by SDS-PAGE. Thereafter, the gels were activated by UV light exposure, and the total protein loaded for each sample was determined using stain-free technology. The activated gel was then electrophoretically transferred to a PVDF membrane. Membrane blocking and incubation were performed as described for whole-muscle homogenate lysates. Membrane staining was visualized by incubation with a high-sensitivity chemiluminescent horseradish peroxidase substrate (SuperSignal West Femto Maximum Sensitivity Substrate, Thermo Fisher Scientific) before image digitalization on ChemiDoc MP. Western blot band intensity was determined by densitometry quantification (total band intensity adjusted for background intensity) and normalized to the total protein loaded as determined by the stain-free method using Image Lab Software v.6.0 (Bio-Rad Laboratories). Analyses were done in technical duplicate, i.e., each sample was loaded twice in adjacent wells, and the average signal intensity was used as the result.

Antibodies. The following antibodies were used: Phospho-Akt (Thr308) (Cell Signaling, catalog no. 9275); Phospho-Akt (Ser473) (Cell Signaling, catalog no. 9271); Akt2 (Cell Signaling, catalog no. 3063); Phospho-GSK-3α/β (Ser21/9) (Cell Signaling, catalog no. 9331); GSK-3β (BD Transduction Laboratories, catalog no. 610202); Phospho-TBC1D4 (Thr642) (Cell Signaling, catalog no. 8881); TBC1D4 (Abcam, catalog no. ab189890); GLUT4 (Thermo Fisher Scientific, catalog no. PA1-1065); Na^+/K^+-adenosine triphosphatase (ATPase) subunit α1 (DSHB, catalog no. α6F); Actin (Sigma-Aldrich, catalog no. A2066); Myc-Tag (Cell Signaling, catalog no. 2272); PRDX2 (Abcam, catalog no. ab109367); PRDX3 (Abcam, catalog no. ab73349); PRDX-$SO_{2/3}$ (Abcam, catalog no. ab16830); 4-HNE (Alpha Diagnostics, catalog no. HNE11-s); Goat Anti-Rabbit Ig, Human ads-HRP (SouthernBiotech, catalog no. 4010-05); and Goat Anti-Mouse Immunoglobulins/HRP (Agilent Technologies, catalog no. P0447).

Muscle mitochondrial bioenergetics

Mitochondrial O_2 consumption and H_2O_2 emission (i.e., production minus removal) rates were simultaneously measured in permeabilized muscle fibers using high-resolution respirometry and fluorometry (Oxygraph O2k-FluoRespirometer; Oroboros Instruments, Innsbruck, Austria).

Preparation of permeabilized muscle fibers and preincubation with mtAO. Upon collection, muscle tissue was dissected free of connective tissue and fat. Multiple small muscle bundles (1.5 to 2.5 mg wet weight) were prepared from each muscle tissue sample. Each bundle was gently teased along the longitudinal axis with needle tip forceps in ice-cold biopsy preservation solution (2.77 mM CaK_2-EGTA, 7.23 mM K_2EGTA, 5.77 mM Na_2ATP, 6.56 mM $MgCl_2$, 20 mM taurine, 15 mM Na_2Phosphocreatine, 20 mM imidazole, 0.5 mM DTT, and 50 mM K-MES, pH 7.1). Teased fiber bundles were treated with saponin (50 μg/ml) for 20 min under gentle rocking on ice to permeabilize the cell membranes while preserving the mitochondrial membranes. Permeabilized fiber bundles (PmFBs) were then transferred to mitochondrial respiration medium [buffer Z: 1 mM EGTA, 5 mM $MgCl_2$, 105 mM K-MES, 30 mM KCl, 10 mM KH_2PO_4, 5 μM pyruvate, 2 μM malate, and BSA (5 mg/ml), pH 7.4] supplemented with either 1 μM decylTPP (i.e., the mitochondria-targeting moiety lacking the antioxidant group) or 1 μM mitoquinone, where they remained for 20 min under gentle rocking on ice, an incubation step allowing for accumulation of decylTPP/mitoquinone into mitochondria, driven by the mitochondrial membrane potential. DecylTPP was used as a control compound to account for the nonspecific effects of mitoquinone on mitochondria (*120*). Thereafter, PmFBs were transferred to a new batch of buffer Z without decylTPP/mitoquinone and rinsed by rocking for 10 min on ice. Then, PmFBs were gently blotted on dry filter paper for 15 s and weighed before being added to an Oxygraph O2k-FluoRespirometer chamber containing 2 ml of buffer Z supplemented with 25 μM blebbistatin, 10 μM Amplex UltraRed, superoxide dismutase (5 U/ml), and horseradish peroxidase (1 U/ml).

Substrate-inhibitor titration protocol. Mitochondrial bioenergetics was determined using a substrate-inhibitor titration protocol validated for simultaneous measurements of mitochondrial O_2 (JO_2) and H_2O_2 (JH_2O_2) fluxes and ADP sensitivity in human PmFBs (*101*). Experiments were conducted in the presence of P-CoA concentrations reflecting normal (20 μM) or high (60 μM) intracellular lipid conditions (*25*, *70*). Specifically, 20 μM P-CoA was titrated in the chambers containing PmFBs pretreated with decylTPP ("Control" sample), whereas 60 μM P-CoA was titrated in the chambers containing PmFBs pretreated with decylTPP ("P-CoA" sample) or mitoquinone ("P-CoA + mtAO" sample) (Fig. 6A). Experiments were performed in duplicates for each condition. The substrate-inhibitor titration protocol started with the addition of succinate (10 mM) to induce reverse electron flow, followed by titration of pyruvate (5 mM) and malate (0.5 mM) to stimulate maximal mitochondrial H_2O_2 emission (Fig. 6B). Thereafter, increasing amounts of ADP (25 to 10,000 μM) were titrated stepwise to determine submaximal mitochondrial H_2O_2 emission rates and the sensitivity of mitochondrial O_2 consumption and H_2O_2 emission to ADP. Glutamate (10 mM) was then titrated to determine maximal OXPHOS capacity through complex I and II, followed by titration of cytochrome C (10 μM) to test mitochondrial outer membrane integrity. Oligomycin (1 μM) was then added to inhibit ATP synthase and measure oligomycin-induced leak respiration ($LEAK_{Omy}$). Last, antimycin A (2.5 μM) was titrated to terminate respiration and allow for correction for nonmitochondrial oxygen consumption.

The sensitivity of mitochondrial O_2 consumption [apparent half-maximal effective concentration (EC_{50})] and H_2O_2 emission [apparent half-maximal inhibitory concentration (IC_{50})] to ADP was estimated using [agonist] versus response (three parameters) analysis and [inhibitor] versus response (three parameters) analysis, respectively, in GraphPad Prism. The first concentration of ADP (25 μM) was not used to estimate the apparent EC_{50} in P-CoA and P-CoA + mtAO, as this concentration of ADP did not stimulate respiration in the presence of 60 μM P-CoA.

Experiments were performed at a chamber temperature of 37°C. Instrumental and chemical O_2 background fluxes were calibrated as a function of O_2 concentration and subtracted from the total volume-specific O_2 flux (Datlab v.7.4 software; Oroboros Instruments). O_2 levels were maintained between 200 and 450 mM to prevent potential O_2 diffusion limitation. Standardized instrumental and chemical calibrations were conducted according to the manufacturer's instructions (Oroboros Instruments, Innsbruck, Austria). These allowed for corrections for (i) background diffusion of O_2 into the chamber, (ii) O_2 solubility in buffer Z, and (iii) background consumption of O_2 by the electrodes, which was determined across the

range (200 to 450 mM) of chamber O_2 concentrations used during the experiments.

Compounds and substrates. The following compounds and substrates were used to evaluate mitochondrial bionergetics: DecylTPP (Santa Cruz Biotechnology, sc-264801); Mitoquinone (gifted by M.P. Murphy, University of Cambridge); Amplex UltraRed (Life Technologies, A36006); superoxide dismutase (Sigma-Aldrich, S 8160); blebbistatin (Sigma-Aldrich, B 0560); horseradish peroxidase (Sigma-Aldrich, P 8250); P-CoA (Sigma-Aldrich, P 9716); succinate (Sigma-Aldrich, S 2378); malate (Sigma-Aldrich, M 1000); ADP (Sigma-Aldrich, A 5285); glutamate (Sigma-Aldrich, G 1626); cytochrome C (Sigma-Aldrich, C 7752); oligomycin (Sigma-Aldrich, O 4876); and antimycin A (Sigma-Aldrich, A 8674).

Enzymatic activity

The maximal enzyme activity of citrate synthase (CS) was quantified in muscle homogenates, as previously described (*100*). Enzymatic activity was normalized to grams of total protein.

Cell studies

Cell culture

L6 rat myoblasts stably expressing *myc*-tagged GLUT4 (L6-GLUT4*myc*) were grown to confluency in α-MEM (Gibco, 22571020) supplemented with 10% fetal bovine serum (FBS) (Sigma-Aldrich, F0804) and 1% antibiotic-antimycotic (Gibco, 15240062). The L6-GLUT4*myc* myoblasts generated by A. Klip's laboratory (SickKids Hospital, Toronto, Canada) were kindly provided by A. Klip. Primary human skeletal muscle (HSKM) myoblasts obtained from m. rectus abdominis of a 17-year-old, nondiabetic male (BMI: 27 kg/m^2) (SK-1111, Donor: P01052-17M, Cook Myosite) were grown to confluency in Myotonic Basal Media (MB-2222) supplemented with 10% Myotonic Growth Supplement (MS-3333) and 1% antibiotic-antimycotic. L6 and HSKM cells were kept at 37°C and in a humidified atmosphere of 5% CO_2.

Cell experiments

L6 myoblast differentiation into myotubes was accomplished by reducing FBS concentration to 2% for 7 days and visually validated by phase contrast microscopy. Seven-day differentiated L6-GLUT4*myc* myotubes seeded in 96-well plates were washed three times in preheated DPBS (Gibco, 14190144) and incubated for 4 hours in BSA vehicle control solution (42 μM, i.e., the highest concentration added with palmitate), palmitate (250 μM; Cayman Chemical, 29558), mitoquinone (50 nM; MedChemExpress, HY-100116A), or combined palmitate and mitoquinone. Dimethyl sulfoxide (DMSO) (0.000001%) served as control for myotubes stimulated with mitoquinone. During the last 15 min of the incubation period, myotubes were stimulated with or without insulin (100 nM). Next, L6 myotubes were washed three times in ice-cold DPBS and fixed in 3% paraformaldehyde before blocking in 5% goat serum (Gibco, 16210064) and incubation with Myc-Tag antibody (1:500 in 5% goat serum). Subsequent incubation in HRP-conjugated secondary antibody allowed for colorimetric detection of plasma membrane–inserted, exofacially exposed GLUT4*myc* using the *o*-phenylenediamine method (*121*).

Differentiation of HSKM myoblasts into myotubes was initiated by switching to differentiation medium comprising α-MEM supplemented with 2% horse serum (Thermo Fisher Scientific, catalog no. 26050-070) and 1% anti-anti. The differentiation medium was replaced every 2 days during the 10 days of differentiation. Ten-day differentiated myotubes maintained in 12-well plates were stimulated for 4 hours with palmitate (250 or 500 μM) or BSA vehicle control solution (42 μM), followed by incubation in 100 mM NEM on ice for 10 min. HSKM myotubes were homogenized in ice-cold lysis buffer [10% glycerol, 1% NP-40, 150 mM NaCl, 50 mM Hepes (pH 7.5), 20 mM sodium pyrophosphate, 10 mM NaF, 20 mM β-glycerophosphate, 2 mM phenylmethylsulfonyl fluoride, 1 mM EDTA (pH 8.0), 1 mM EGTA (pH 8.0), 2 mM Na_3VO_4, leupeptin (10 μg/ml), aprotinin (10 μg/ml), 3 mM benzamidine] containing 100 mM NEM. Each sample was sonicated for 15 s (10% intensity, Q2000 Qsonica sonicator) and the lysate supernatants were collected after centrifugation at 18,320*g* for 20 min at 4°C.

Animal studies

Animals

Animal experiments were approved by the Danish Animal Experimental Inspectorate (reference no. 2014-15-2934-01037) and complied with the European Union legislation outlined by the European Directive 2010/63/EU. To determine the effect of mtROS on insulin-stimulated GLUT4 accumulation at the plasma membrane, the pB-GLUT4-7*myc*-GFP construct (Jonathan Bogan, Addgene, Plasmid no. 52872) was expressed in skeletal muscle of male C57BL/6N mice at 12 to 14 weeks of age.

Animal experiments

In vivo gene transfer in mouse skeletal muscle. Skeletal muscle electroporation was performed in FDB muscles as previously described (*61*). Male C57BL/6N mice 12 to 14 weeks of age were anesthetized by 2 to 3% isoflurane inhalation and injected into the foot sole with 10 μl of hyaluronidase (0.36 mg/ml; Sigma, H3884) diluted in PBS. After 60 min, 20 μl of sterile saline containing 20 μg of DNA was injected at the same location. Electroporation of the FDB muscle was performed by delivering 15 20-ms pulses at 1 Hz at an electrical field strength of 75 V/cm using acupuncture needles (0.20 × 25 mm, Tai Chi, Lhasa OMS) connected to an ECM 830 BTX electroporator (BTX Harvard Apparatus). After the procedure, the animals were transferred back to their cages and allowed to recover for at least 7 days.

Fiber isolation and GLUT4 translocation assay. Mice were euthanized by cervical dislocation, and FDB was quickly removed under a dissection microscope. Muscles were incubated in serum-free alpha-Minimum Essential Medium Eagle (α-MEM) containing collagenase type 1 (2.0 mg/ml) from *Clostridium histolyticum* (Sigma-Aldrich, C0130) for 2 hours at 37°C. After collagenase treatment, muscles were incubated in 2 ml of α-MEM containing 5% horse serum (Gibco, 26050-70), followed by mechanical dissociation of individual muscle fibers using fire-polished Pasteur pipettes. Pooled fibers were seeded on 13-mm-diameter glass coverslips (Hounissen) coated with Engelbreth-Holm-Swarm murine sarcoma ECM gel (Merck, E1270). After 1 hour, 1 ml of α-MEM containing 5% fetal bovine serum was added to the wells, and the muscle fibers were cultured overnight. The following day, muscle fibers were maintained in serum-free α-MEM for 4 hours containing either vehicle (0.1% ethanol) or 10 μM MitoPQ (Abcam, ab146819) and stimulated with either saline or 100 nM insulin for 20 min. Muscle fibers were fixed in 4% paraformaldehyde (4% PFA) diluted in PBS for 10 min. PFA-fixed muscle fibers were washed 3×10 min in PBS and incubated in blocking buffer [1% BSA, 5% goat serum (Gibco, 16210-064), and 0.1% sodium azide (Merck, 247-852)] for 1 hour. The muscle fibers were then incubated overnight with an antibody against the *myc* tag diluted 1:400 in blocking buffer. The next day, the fibers were washed 3 × 10 min

in PBS containing 0.04% saponin and incubated with Alexa Flour 568 antibody (Life Technologies, catalog no. A10042) in blocking buffer containing 0.04% saponin for 2 hours. Last, the fibers were washed three times, each for 10 min, in PBS and mounted on glass slides in Vectashield (Vector Laboratories, H-1000).

Live imaging procedures. Images were collected using a 40× 1.2 NA (numerical aperture) oil immersion objective on an LSM 980 confocal microscope (Zeiss) driven by Zeiss Zen Blue 3. To determine the fraction of GLUT4 accumulated on the plasma membrane surface, both GFP and *myc* signals were quantified as previously described (*61*). Briefly, the *myc* and GFP channels were duplicated, and the new images underwent background subtraction and Gaussian blur adjustment (radius = 2) and were made binary. From these binary images, regions of positive GFP and *myc* signals were selected and overlaid onto the original images for quantification of the integrated density of GFP and *myc* signals, respectively.

Statistical analysis

For clamp-based outcomes, muscle insulin signaling, and muscle redox state, between-treatment differences (Lipid versus Lipid + mtAO) were determined using a linear mixed model including treatment as a fixed factor, participants as a random factor, and with an unstructured covariance pattern. Within-treatment differences (i.e., Baseline versus End-clamp or Pre-clamp versus End-clamp) were determined using a linear mixed model with treatment-time interaction as a fixed factor, participants as a random factor, and with an unstructured covariance pattern. To adjust for the period effects associated with the crossover design of the study, a period variable was included as a fixed factor in the linear mixed models. For mitochondrial bioenergetics, between-treatment differences (Control versus P-CoA versus P-CoA + mtAO) were determined using a linear mixed model with treatment as a fixed factor and participants as a random factor. For all analyses, model checking was based on Shapiro-Wilk's test and quantile-quantile (Q-Q) plots. In case of heteroscedasticity (i.e., unequal variance), log transformation was applied before analysis. *P* values were evaluated using Kenward-Roger approximation of the degrees of freedom. Analyses were performed using SAS Enterprise Guide version 7.15.

For rodent muscle cell and fiber experiments, as well as for indices of mitochondrial ADP sensitivity (EC_{50} and IC_{50}) in human PmFBs, a one-way analysis of variance (ANOVA) in GraphPad Prism was used to estimate between-treatment differences.

The level of significance for all analyses was set at $P < 0.05$. Data are graphically presented as observed individual values with model-based estimated means ±95% confidence limits, unless otherwise stated.

Supplementary Materials

This PDF file includes:

Figs. S1 and S2

Uncropped Western blots

REFERENCES AND NOTES

1. R. A. DeFronzo, E. Jacot, E. Jequier, E. Maeder, J. Wahren, J. P. Felber, The effect of insulin on the disposal of intravenous glucose: Results from indirect calorimetry and hepatic and femoral venous catheterization. *Diabetes* **30**, 1000–1007 (1981).
2. M. Roden, G. I. Shulman, The integrative biology of type 2 diabetes. *Nature* **576**, 51–60 (2019).
3. M. C. Petersen, G. I. Shulman, Mechanisms of insulin action and insulin resistance. *Physiol. Rev.* **98**, 2133–2223 (2018).
4. J. Szendroedi, E. Phielix, M. Roden, The role of mitochondria in insulin resistance and type 2 diabetes mellitus. *Nat. Rev. Endocrinol.* **8**, 92–103 (2012).
5. B. B. Lowell, G. I. Shulman, Mitochondrial dysfunction and type 2 diabetes. *Science* **307**, 384–387 (2005).
6. S. Ghosh, S. E. Wicks, B. Vandanmagsar, T. M. Mendoza, D. S. Bayless, J. M. Salbaum, S. P. Dearth, S. R. Campagna, R. L. Mynatt, R. C. Noland, Extensive metabolic remodeling after limiting mitochondrial lipid burden is consistent with an improved metabolic health profile. *J. Biol. Chem.* **294**, 12313–12327 (2019).
7. T. R. Koves, J. R. Ussher, R. C. Noland, D. Slentz, M. Mosedale, O. Ilkayeva, J. Bain, R. Stevens, J. R. B. Dyck, C. B. Newgard, G. D. Lopaschuk, D. M. Muoio, Mitochondrial overload and incomplete fatty acid oxidation contribute to skeletal muscle insulin resistance. *Cell Metab.* **7**, 45–56 (2008).
8. P. D. Neufer, Cutting fuel offers new clues in diabetic mystery. *J. Biol. Chem.* **294**, 12328–12329 (2019).
9. S. E. Wicks, B. Vandanmagsar, K. R. Haynie, S. E. Fuller, J. D. Warfel, J. M. Stephens, M. Wang, X. Han, J. Zhang, R. C. Noland, R. L. Mynatt, Impaired mitochondrial fat oxidation induces adaptive remodeling of muscle metabolism. *Proc. Natl. Acad. Sci. U.S.A.* **112**, E3300–E3309 (2015).
10. C. Koliaki, M. Roden, Alterations of mitochondrial function and insulin sensitivity in human obesity and diabetes mellitus. *Annu. Rev. Nutr.* **36**, 337–367 (2016).
11. J. O. Holloszy, "Deficiency" of mitochondria in muscle does not cause insulin resistance. *Diabetes* **62**, 1036–1040 (2013).
12. B. H. Goodpaster, Mitochondrial deficiency is associated with insulin resistance. *Diabetes* **62**, 1032–1035 (2013).
13. D. M. Muoio, P. D. Neufer, Lipid-induced mitochondrial stress and insulin action in muscle. *Cell Metab.* **15**, 595–605 (2012).
14. G. S. Shadel, T. L. Horvath, Mitochondrial ROS signaling in organismal homeostasis. *Cell* **163**, 560–569 (2015).
15. H. Sies, C. Berndt, D. P. Jones, Oxidative stress. *Annu. Rev. Biochem.* **86**, 715–748 (2017).
16. H. Sies, Oxidative eustress: On constant alert for redox homeostasis. *Redox Biol.* **41**, 101867 (2021).
17. N. Houstis, E. D. Rosen, E. S. Lander, Reactive oxygen species have a causal role in multiple forms of insulin resistance. *Nature* **440**, 944–948 (2006).
18. E. L. Seifert, C. Estey, J. Y. Xuan, M.-E. Harper, Electron transport chain-dependent and -independent mechanisms of mitochondrial H_2O_2 emission during long-chain fatty acid oxidation. *J. Biol. Chem.* **285**, 5748–5758 (2010).
19. J. V. Rodrigues, C. M. Gomes, Mechanism of superoxide and hydrogen peroxide generation by human electron-transfer flavoprotein and pathological variants. *Free Radic. Biol. Med.* **53**, 12–19 (2012).
20. J. St-Pierre, J. A. Buckingham, S. J. Roebuck, M. D. Brand, Topology of superoxide production from different sites in the mitochondrial electron transport chain. *J. Biol. Chem.* **277**, 44784–44790 (2002).
21. E. J. Anderson, H. Yamazaki, P. D. Neufer, Induction of endogenous uncoupling protein 3 suppresses mitochondrial oxidant emission during fatty acid-supported respiration. *J. Biol. Chem.* **282**, 31257–31266 (2007).
22. K. H. Fisher-Wellman, P. D. Neufer, Linking mitochondrial bioenergetics to insulin resistance via redox biology. *Trends Endocrinol. Metab.* **23**, 142–153 (2012).
23. A. Diaz-Vegas, S. Madsen, K. C. Cooke, L. Carroll, J. X. Khor, N. Turner, X. Y. Lim, M. A. Astore, J. C. Morris, A. S. Don, A. Garfield, S. Zarini, K. A. Zemski Berry, A. P. Ryan, B. C. Bergman, J. T. Brozinick, D. E. James, J. G. Burchfield, Mitochondrial electron transport chain, ceramide, and coenzyme Q are linked in a pathway that drives insulin resistance in skeletal muscle. *eLife* **12**, RP87340 (2023).
24. A. Ludzki, S. Paglialunga, B. K. Smith, E. A. Herbst, M. K. Allison, G. J. Heigenhauser, P. D. Neufer, G. P. Holloway, Rapid repression of ADP transport by palmitoyl-CoA is attenuated by exercise training in humans: A potential mechanism to decrease oxidative stress and improve skeletal muscle insulin signaling. *Diabetes* **64**, 2769–2779 (2015).
25. P. M. Miotto, P. J. LeBlanc, G. P. Holloway, High-fat diet causes mitochondrial dysfunction as a result of impaired ADP sensitivity. *Diabetes* **67**, 2199–2205 (2018).
26. D. E. James, J. Stöckli, M. J. Birnbaum, The aetiology and molecular landscape of insulin resistance. *Nat. Rev. Mol. Cell Biol.* **22**, 751–771 (2021).
27. D. J. Fazakerley, J. R. Krycer, A. L. Kearney, S. L. Hocking, D. E. James, Muscle and adipose tissue insulin resistance: Malady without mechanism? *J. Lipid Res.* **60**, 1720–1732 (2019).
28. E. J. Anderson, M. E. Lustig, K. E. Boyle, T. L. Woodlief, D. A. Kane, C.-T. Lin, J. W. Price III, L. Kang, P. S. Rabinovitch, H. H. Szeto, J. A. Houmard, R. N. Cortright, D. H. Wasserman, P. D. Neufer, Mitochondrial H_2O_2 emission and cellular redox state link excess fat intake to insulin resistance in both rodents and humans. *J. Clin. Investig.* **119**, 573–581 (2009).
29. D. S. Lark, L. Kang, M. E. Lustig, J. S. Bonner, F. D. James, P. D. Neufer, D. H. Wasserman, Enhanced mitochondrial superoxide scavenging does not improve muscle insulin action in the high fat-fed mouse. *PLOS ONE* **10**, e0126732 (2015).
30. K. L. Hoehn, A. B. Salmon, C. Hohnen-Behrens, N. Turner, A. J. Hoy, G. J. Maghzal, R. Stocker, H. Van Remmen, E. W. Kraegen, G. J. Cooney, A. R. Richardson, D. E. James,

Insulin resistance is a cellular antioxidant defense mechanism. *Proc. Natl. Acad. Sci. U.S.A* **106**, 17787–17792 (2009).
31. H.-Y. Lee, J. S. Lee, T. Alves, W. Ladiges, P. S. Rabinovitch, M. J. Jurczak, C. S. Choi, G. I. Shulman, V. T. Samuel, Mitochondrial-targeted catalase protects against high-fat diet–induced muscle insulin resistance by decreasing intramuscular lipid accumulation. *Diabetes* **66**, 2072–2081 (2017).
32. G. F. Kelso, C. M. Porteous, C. V. Coulter, G. Hughes, W. K. Porteous, E. C. Ledgerwood, R. A. J. Smith, M. P. Murphy, Selective targeting of a redox-active ubiquinone to mitochondria within cells: Antioxidant and antiapoptotic properties. *J. Biol. Chem.* **276**, 4588–4596 (2001).
33. A. V. Birk, W. M. Chao, C. Bracken, J. D. Warren, H. H. Szeto, Targeting mitochondrial cardiolipin and the cytochrome c/cardiolipin complex to promote electron transport and optimize mitochondrial ATP synthesis. *Br. J. Pharmacol.* **171**, 2017–2028 (2014).
34. C. Feillet-Coudray, G. Fouret, R. Ebabe Elle, J. Rieusset, B. Bonafos, B. Chabi, D. Crouzier, K. Zarkovic, N. Zarkovic, J. Ramos, E. Badia, M. P. Murphy, J. P. Cristol, C. Coudray, The mitochondrial-targeted antioxidant MitoQ ameliorates metabolic syndrome features in obesogenic diet-fed rats better than Apocynin or Allopurinol. *Free Radic. Res.* **48**, 1232–1246 (2014).
35. D. J. Fazakerley, A. Y. Minard, J. R. Krycer, K. C. Thomas, J. Stöckli, D. J. Harney, J. G. Burchfield, G. J. Maghzal, S. T. Caldwell, R. C. Hartley, R. Stocker, M. P. Murphy, D. E. James, Mitochondrial oxidative stress causes insulin resistance without disrupting oxidative phosphorylation. *J. Biol. Chem.* **293**, 7315–7328 (2018).
36. K. McKeegan, S. A. Mason, A. J. Trewin, M. A. Keske, G. D. Wadley, P. A. Della Gatta, M. G. Nikolaidis, L. Parker, Reactive oxygen species in exercise and insulin resistance: Working towards personalized antioxidant treatment. *Redox Biol.* **44**, 102005 (2021).
37. D. J. Drucker, Never waste a good crisis: Confronting reproducibility in translational research. *Cell Metab.* **24**, 348–360 (2016).
38. V. T. Samuel, K. F. Petersen, G. I. Shulman, Lipid-induced insulin resistance: Unravelling the mechanism. *Lancet* **375**, 2267–2277 (2010).
39. R. Belfort, L. Mandarino, S. Kashyap, K. Wirfel, T. Pratipanawatr, R. Berria, R. A. Defronzo, K. Cusi, Dose-response effect of elevated plasma free fatty acid on insulin signaling. *Diabetes* **54**, 1640–1648 (2005).
40. R. Barazzoni, M. Zanetti, G. G. Cappellari, A. Semolic, M. Boschelle, E. Codarin, A. Pirulli, L. Cattin, G. Guarnieri, Fatty acids acutely enhance insulin-induced oxidative stress and cause insulin resistance by increasing mitochondrial reactive oxygen species (ROS) generation and nuclear factor-κB inhibitor (IκB)-nuclear factor-κB (NFκB) activation in rat muscle, in the absence of mitochondrial dysfunction. *Diabetologia* **55**, 773–782 (2012).
41. R. Weiss, S. Dufour, S. E. Taksali, W. V. Tamborlane, K. F. Petersen, R. C. Bonadonna, L. Boselli, G. Barbetta, K. Allen, F. Rife, M. Savoye, J. Dziura, R. Sherwin, G. I. Shulman, S. Caprio, Prediabetes in obese youth: A syndrome of impaired glucose tolerance, severe insulin resistance, and altered myocellular and abdominal fat partitioning. *Lancet* **362**, 951–957 (2003).
42. K. H. Fisher-Wellman, T. M. Weber, B. L. Cathey, P. M. Brophy, L. A. Gilliam, C. L. Kane, J. M. Maples, T. P. Gavin, J. A. Houmard, P. D. Neufer, Mitochondrial respiratory capacity and content are normal in young insulin-resistant obese humans. *Diabetes* **63**, 132–141 (2014).
43. L. D. Høeg, K. A. Sjøberg, J. Jeppesen, T. E. Jensen, C. Frøsig, J. B. Birk, B. Bisiani, N. Hiscock, H. Pilegaard, J. F. P. Wojtaszewski, E. A. Richter, B. Kiens, Lipid-induced insulin resistance affects women less than men and is not accompanied by inflammation or impaired proximal insulin signaling. *Diabetes* **60**, 64–73 (2011).
44. C. Pehmøller, N. Brandt, J. B. Birk, L. D. Høeg, K. A. Sjøberg, L. J. Goodyear, B. Kiens, E. A. Richter, J. F. P. Wojtaszewski, Exercise alleviates lipid-induced insulin resistance in human skeletal muscle-signaling interaction at the level of TBC1 domain family member 4. *Diabetes* **61**, 2743–2752 (2012).
45. G. Boden, X. Chen, Effects of fat on glucose uptake and utilization in patients with non-insulin-dependent diabetes. *J. Clin. Invest.* **96**, 1261–1268 (1995).
46. S.-Y. Park, E. J. Pekas, R. J. Headid, W.-M. Son, T. K. Wooden, J. Song, G. Layec, S. K. Yadav, P. K. Mishra, I. I. Pipinos, Acute mitochondrial antioxidant intake improves endothelial function, antioxidant enzyme activity, and exercise tolerance in patients with peripheral artery disease. *Am. J. Physiol. Heart Circ. Physiol.* **319**, H456–H467 (2020).
47. M. J. Rossman, J. R. Santos-Parker, C. A. C. Steward, N. Z. Bispham, L. M. Cuevas, H. L. Rosenberg, K. A. Woodward, M. Chonchol, R. A. Gioscia-Ryan, M. P. Murphy, D. R. Seals, Chronic supplementation with a mitochondrial antioxidant (MitoQ) improves vascular function in healthy older adults. *Hypertension* **71**, 1056–1063 (2018).
48. A. D. Baron, H. O. Steinberg, H. Chaker, R. Leaming, A. Johnson, G. Brechtel, Insulin-mediated skeletal muscle vasodilation contributes to both insulin sensitivity and responsiveness in lean humans. *J. Clin. Invest.* **96**, 786–792 (1995).
49. H. O. Steinberg, M. Tarshoby, R. Monestel, G. Hook, J. Cronin, A. Johnson, B. Bayazeed, A. D. Baron, Elevated circulating free fatty acid levels impair endothelium-dependent vasodilation. *J. Clin. Invest.* **100**, 1230–1239 (1997).
50. D. E. Kelley, B. Goodpaster, R. R. Wing, J. A. Simoneau, Skeletal muscle fatty acid metabolism in association with insulin resistance, obesity, and weight loss. *Am. J. Physiol.* **277**, E1130–E1141 (1999).
51. J. D. Song, T. C. Alves, D. E. Befroy, R. J. Perry, G. F. Mason, X. Zhang, A. Munk, Y. Zhang, D. Zhang, G. W. Cline, D. L. Rothman, K. F. Petersen, G. I. Shulman, Dissociation of muscle insulin resistance from alterations in mitochondrial substrate preference. *Cell Metab.* **32**, 726–735.e5 (2020).
52. S. I. Itani, N. B. Ruderman, F. Schmieder, G. Boden, Lipid-induced insulin resistance in human muscle is associated with changes in diacylglycerol, protein kinase C, and IκB-α. *Diabetes* **51**, 2005–2011 (2002).
53. S. I. Itani, Q. Zhou, W. J. Pories, K. G. MacDonald, G. L. Dohm, Involvement of protein kinase C in human skeletal muscle insulin resistance and obesity. *Diabetes* **49**, 1353–1358 (2000).
54. A. Dresner, D. Laurent, M. Marcucci, M. E. Griffin, S. Dufour, G. W. Cline, L. A. Slezak, D. K. Andersen, R. S. Hundal, D. L. Rothman, K. F. Petersen, G. I. Shulman, Effects of free fatty acids on glucose transport and IRS-1–associated phosphatidylinositol 3-kinase activity. *J. Clin. Invest.* **103**, 253–259 (1999).
55. J. Szendroedi, T. Yoshimura, E. Phielix, C. Koliaki, M. Marcucci, D. Zhang, T. Jelenik, J. Müller, C. Herder, P. Nowotny, G. I. Shulman, M. Roden, Role of diacylglycerol activation of PKCθ in lipid-induced muscle insulin resistance in humans. *Proc. Natl. Acad. Sci. U.S.A.* **111**, 9597–9602 (2014).
56. A. J. Hoy, A. E. Brandon, N. Turner, M. J. Watt, C. R. Bruce, G. J. Cooney, E. W. Kraegen, Lipid and insulin infusion-induced skeletal muscle insulin resistance is likely due to metabolic feedback and not changes in IRS-1, Akt, or AS160 phosphorylation. *Am J. Physiol. Endocrinol. Metab.* **297**, E67–E75 (2009).
57. H. Storgaard, C. B. Jensen, M. Björnholm, X. M. Song, S. Madsbad, J. R. Zierath, A. A. Vaag, Dissociation between fat-induced in vivo insulin resistance and proximal insulin signaling in skeletal muscle in men at risk for type 2 diabetes. *J. Clin. Endocrinol. Metab.* **89**, 1301–1311 (2004).
58. J. J. Dubé, P. M. Coen, G. Distefano, A. C. Chacon, N. L. Helbling, M. E. Desimone, M. Stafanovic-Racic, K. C. Hames, A. A. Despines, F. G. S. Toledo, B. H. Goodpaster, Effects of acute lipid overload on skeletal muscle insulin resistance, metabolic flexibility, and mitochondrial performance. *Am. J. Physiol. Endocrinol. Metab.* **307**, E1117–E1124 (2014).
59. K. Tsintzas, K. Chokkalingam, K. Jewell, L. Norton, I. A. Macdonald, D. Constantin-Teodosiu, Elevated free fatty acids attenuate the insulin-induced suppression of PDK4 gene expression in human skeletal muscle: Potential role of intramuscular long-chain acyl-coenzyme A. *J. Clin. Endocrinol. Metab.* **92**, 3967–3972 (2007).
60. J. R. Zierath, L. He, A. Gumà, E. O. Wahlström, A. Klip, H. Wallberg-Henriksson, Insulin action on glucose transport and plasma membrane GLUT4 content in skeletal muscle from patients with NIDDM. *Diabetologia* **39**, 1180 (1996).
61. J. R. Knudsen, C. Henriquez-Olguin, Z. Li, T. E. Jensen, Electroporated GLUT4-7*myc*-GFP detects in vivo glucose transporter 4 translocation in skeletal muscle without discernible changes in GFP patterns. *Exp. Physiol.* **104**, 704–714 (2019).
62. R. A. Poynton, M. B. Hampton, Peroxiredoxins as biomarkers of oxidative stress. *Biochim. Biophys. Acta* **1840**, 906–912 (2014).
63. R. Ch, G. Rey, S. Ray, P. K. Jha, P. C. Driscoll, M. S. Dos Santos, D. M. Malik, R. Lach, A. M. Weljie, J. I. MacRae, U. K. Valekunja, A. B. Reddy, Rhythmic glucose metabolism regulates the redox circadian clockwork in human red blood cells. *Nat. Commun.* **12**, 377 (2021).
64. J. S. O'Neill, A. B. Reddy, Circadian clocks in human red blood cells. *Nature* **469**, 498–503 (2011).
65. J. Williamson, C. M. Hughes, J. N. Cobley, G. W. Davison, The mitochondria-targeted antioxidant MitoQ, attenuates exercise-induced mitochondrial DNA damage. *Redox Biol.* **36**, 101673 (2020).
66. P. Dandona, A. Aljada, P. Mohanty, H. Ghanim, W. Hamouda, E. Assian, S. Ahmad, Insulin inhibits intranuclear nuclear factor κB and stimulates IκB in mononuclear cells in obese subjects: Evidence for an anti-inflammatory effect? *J. Clin. Endocrinol. Metab.* **86**, 3257–3265 (2001).
67. L. Monnier, C. Colette, E. Mas, F. Michel, J. P. Cristol, C. Boegner, D. R. Owens, Regulation of oxidative stress by glycaemic control: Evidence for an independent inhibitory effect of insulin therapy. *Diabetologia* **53**, 562–571 (2010).
68. H. S. Brunetta, H. L. Petrick, B. Vachon, E. A. Nunes, G. P. Holloway, Insulin rapidly increases skeletal muscle mitochondrial ADP sensitivity in the absence of a high lipid environment. *Biochem. J.* **478**, 2539–2553 (2021).
69. A. Ceriello, A. Novials, S. Canivell, L. La Sala, G. Pujadas, K. Esposito, R. Testa, L. Bucciarelli, M. Rondinelli, S. Genovese, Simultaneous GLP-1 and insulin administration acutely enhances their vasodilatory, antiinflammatory, and antioxidant action in type 2 diabetes. *Diabetes Care* **37**, 1938–1943 (2014).
70. B. A. Ellis, A. Poynten, A. J. Lowy, S. M. Furler, D. J. Chisholm, E. W. Kraegen, G. J. Cooney, Long-chain acyl-CoA esters as indicators of lipid metabolism and insulin sensitivity in rat and human muscle. *Am. J. Physiol. Endocrinol. Metab.* **279**, E554–E560 (2000).

71. I. T. Mak, J. H. Kramer, W. B. Weglicki, Potentiation of free radical-induced lipid peroxidative injury to sarcolemmal membranes by lipid amphiphiles. *J. Biol. Chem.* **261**, 1153–1157 (1986).
72. H. Tominaga, H. Katoh, K. Odagiri, Y. Takeuchi, H. Kawashima, M. Saotome, T. Urushida, H. Satoh, H. Hayashi, Different effects of palmitoyl-$_L$-carnitine and palmitoyl-CoA on mitochondrial function in rat ventricular myocytes. *Am. J. Physiol. Heart Circ. Physiol.* **295**, H105–H112 (2008).
73. A. Guarás, E. Perales-Clemente, E. Calvo, R. Acín-Pérez, M. Loureiro-Lopez, C. Pujol, I. Martínez-Carrascoso, E. Nuñez, F. García-Marqués, M. A. Rodríguez-Hernández, A. Cortés, F. Diaz, A. Pérez-Martos, C. T. Moraes, P. Fernández-Silva, A. Trifunovic, P. Navas, J. Vazquez, J. A. Enríquez, The $CoQH_2$/CoQ ratio serves as a sensor of respiratory chain efficiency. *Cell Rep.* **15**, 197–209 (2016).
74. P.-A. Barbeau, P. M. Miotto, G. P. Holloway, Mitochondrial-derived reactive oxygen species influence ADP sensitivity, but not CPT-I substrate sensitivity. *Biochem. J.* **475**, 2997–3008 (2018).
75. G. Pharaoh, J. Brown, R. Ranjit, Z. Ungvari, H. Van Remmen, Reduced adenosine diphosphate sensitivity in skeletal muscle mitochondria increases reactive oxygen species production in mouse models of aging and oxidative stress but not denervation. *JCSM Rapid Commun.* **4**, 75–89 (2021).
76. M. A. Abdul-Ghani, R. Jani, A. Chavez, M. Molina-Carrion, D. Tripathy, R. A. DeFronzo, Mitochondrial reactive oxygen species generation in obese non-diabetic and type 2 diabetic participants. *Diabetologia* **52**, 574–582 (2009).
77. B. Nowotny, L. Zahiragic, D. Krog, P. J. Nowotny, C. Herder, M. Carstensen, T. Yoshimura, J. Szendroedi, E. Phielix, P. Schadewaldt, N. C. Schloot, G. I. Shulman, M. Roden, Mechanisms underlying the onset of oral lipid–induced skeletal muscle insulin resistance in humans. *Diabetes* **62**, 2240–2248 (2013).
78. L. Kang, M. E. Lustig, J. S. Bonner, R. S. Lee-Young, W. H. Mayes, F. D. James, C. T. Lin, C. G. R. Perry, E. J. Anderson, P. D. Neufer, D. H. Wasserman, Mitochondrial antioxidative capacity regulates muscle glucose uptake in the conscious mouse: Effect of exercise and diet. *J. Appl. Physiol.* **113**, 1173–1183 (2012).
79. M. J. Boden, A. E. Brandon, J. D. Tid-Ang, E. Preston, D. Wilks, E. Stuart, M. E. Cleasby, N. Turner, G. J. Cooney, E. W. Kraegen, Overexpression of manganese superoxide dismutase ameliorates high-fat diet-induced insulin resistance in rat skeletal muscle. *Am. J. Physiol. Endocrinol. Metab.* **303**, E798–E805 (2012).
80. L. Chen, R. Na, M. Gu, A. B. Salmon, Y. Liu, H. Liang, W. Qi, H. Van Remmen, A. Richardson, Q. Ran, Reduction of mitochondrial H_2O_2 by overexpressing peroxiredoxin 3 improves glucose tolerance in mice. *Aging Cell* **7**, 866–878 (2008).
81. H.-Y. Lee, C. S. Choi, A. L. Birkenfeld, T. C. Alves, F. R. Jornayvaz, M. J. Jurczak, D. Zhang, D. K. Woo, G. S. Shadel, W. Ladiges, P. S. Rabinovitch, J. H. Santos, K. F. Petersen, V. T. Samuel, G. I. Shulman, Targeted expression of catalase to mitochondria prevents age-associated reductions in mitochondrial function and insulin resistance. *Cell Metab.* **12**, 668–674 (2010).
82. G. Marín-Royo, C. Rodríguez, A. L. Pape, R. Jurado-Lopez, M. Luaces, A. Antequera, J. Martínez-Gonzalez, F. V. Souza-Neto, M. L. Nieto, E. Martínez-Martínez, V. Cachofeiro, The role of mitochondrial oxidative stress in the metabolic alterations in diet-induced obesity in rats. *FASEB J.* **33**, 12060–12072 (2019).
83. G. Fouret, E. Tolika, J. Lecomte, B. Bonafos, M. Aoun, M. P. Murphy, C. Ferreri, C. Chatgilialoglu, E. Dubreucq, C. Coudray, C. Feillet-Coudray, The mitochondrial-targeted antioxidant, MitoQ, increases liver mitochondrial cardiolipin content in obesogenic diet-fed rats. *Biochim. Biophys. Acta* **1847**, 1025–1035 (2015).
84. C. Coudray, G. Fouret, K. Lambert, C. Ferreri, J. Rieusset, A. Blachnio-Zabielska, J. Lecomte, R. Ebabe Elle, E. Badia, M. P. Murphy, C. Feillet-Coudray, A mitochondrial-targeted ubiquinone modulates muscle lipid profile and improves mitochondrial respiration in obesogenic diet-fed rats. *Br. J. Nutr.* **115**, 1155–1166 (2016).
85. J. R. Mercer, E. Yu, N. Figg, K. K. Cheng, T. A. Prime, J. L. Griffin, M. Masoodi, A. Vidal-Puig, M. P. Murphy, M. R. Bennett, The mitochondria-targeted antioxidant MitoQ decreases features of the metabolic syndrome in $ATM^{+/-}$/$ApoE^{-/-}$ mice. *Free Radic. Biol. Med.* **52**, 841–849 (2012).
86. E. M. Jeong, J. Chung, H. Liu, Y. Go, S. Gladstein, A. Farzaneh-Far, E. D. Lewandowski, S. C. Dudley, Role of mitochondrial oxidative stress in glucose tolerance, insulin resistance, and cardiac diastolic dysfunction. *J. Am. Heart Assoc.* **5**, e003046 (2016).
87. T. Pham, C. L. Macrae, S. C. Broome, F. D. Randall, R. Narang, H. W. Wang, T. A. Mori, A. J. R. Hickey, C. J. Mitchell, T. L. Merry, MitoQ and CoQ10 supplementation mildly suppresses skeletal muscle mitochondrial hydrogen peroxide levels without impacting mitochondrial function in middle-aged men. *Eur. J. Appl. Physiol.* **120**, 1657–1669 (2020).
88. K. Yoshida, T. Shimizugawa, M. Ono, H. Furukawa, Angiopoietin-like protein 4 is a potent hyperlipidemia-inducing factor in mice and inhibitor of lipoprotein lipase. *J. Lipid Res.* **43**, 1770–1772 (2002).
89. A. Xu, M. C. Lam, K. W. Chan, Y. Wang, J. Zhang, R. L. C. Boo, J. Y. Xu, B. Chen, W. S. Chow, A. W. K. Tso, K. S. L. Lam, Angiopoietin-like protein 4 decreases blood glucose and improves glucose tolerance but induces hyperlipidemia and hepatic steatosis in mice. *Proc. Natl. Acad. Sci. U.S.A.* **102**, 6086–6091 (2005).
90. S. Mandard, F. Zandbergen, E. van Straten, W. Wahli, F. Kuipers, M. Müller, S. Kersten, The fasting-induced adipose factor/angiopoietin-like protein 4 is physically associated with lipoproteins and governs plasma lipid levels and adiposity. *J. Biol. Chem.* **281**, 934–944 (2006).
91. R. Choudhuri, A. L. Sowers, G. V. R. Chandramouli, J. Gamson, M. C. Krishna, J. B. Mitchell, J. A. Cook, The antioxidant tempol transforms gut microbiome to resist obesity in female C3H mice fed a high fat diet. *Free Radic. Biol. Med.* **178**, 380–390 (2022).
92. P. J. Randle, P. B. Garland, C. N. Hales, E. A. Newsholme, The glucose fatty-acid cycle its role in insulin sensitivity and the metabolic disturbances of diabetes mellitus. *Lancet* **281**, 785–789 (1963).
93. M. Straczkowski, I. Kowalska, A. Nikolajuk, S. Dzienis-Straczkowska, I. Kinalska, M. Baranowski, M. Zendzian-Piotrowska, Z. Brzezinska, J. Gorski, Relationship between insulin sensitivity and sphingomyelin signaling pathway in human skeletal muscle. *Diabetes* **53**, 1215–1221 (2004).
94. M. J. Serlie, A. J. Meijer, J. E. Groener, M. Duran, E. Endert, E. Fliers, J. M. Aerts, H. P. Sauerwein, Short-term manipulation of plasma free fatty acids does not change skeletal muscle concentrations of ceramide and glucosylceramide in lean and overweight subjects. *J. Clin. Endocrinol. Metab.* **92**, 1524–1529 (2007).
95. C. L. Axelrod, C. E. Fealy, M. L. Erickson, G. Davuluri, H. Fujioka, W. S. Dantas, E. Huang, K. Pergola, J. T. Mey, W. T. King, A. Mulya, D. Hsia, B. Burguera, B. Tandler, C. L. Hoppel, J. P. Kirwan, Lipids activate skeletal muscle mitochondrial fission and quality control networks to induce insulin resistance in humans. *Metabolism* **121**, 154803 (2021).
96. E. A. Richter, Is GLUT4 translocation the answer to exercise-stimulated muscle glucose uptake? *Am. J. Physiol. Endocrinol. Metab.* **320**, E240–E243 (2021).
97. J. Li, C. Romestaing, X. Han, Y. Li, X. Hao, Y. Wu, C. Sun, X. Liu, L. S. Jefferson, J. Xiong, K. F. Lanoue, Z. Chang, C. J. Lynch, H. Wang, Y. Shi, Cardiolipin remodeling by ALCAT1 links oxidative stress and mitochondrial dysfunction to obesity. *Cell Metab.* **12**, 154–165 (2010).
98. D. B. Zorov, M. Juhaszova, S. J. Sollott, Mitochondrial reactive oxygen species (ROS) and ROS-induced ROS release. *Physiol. Rev.* **94**, 909–950 (2014).
99. G. K. Sakellariou, T. Pearson, A. P. Lightfoot, G. A. Nye, N. Wells, I. I. Giakoumaki, R. D. Griffiths, A. McArdle, M. J. Jackson, Long-term administration of the mitochondria-targeted antioxidant mitoquinone mesylate fails to attenuate age-related oxidative damage or rescue the loss of muscle mass and function associated with aging of skeletal muscle. *FASEB J.* **30**, 3771–3785 (2016).
100. M. Fiorenza, A. K. Lemminger, M. Marker, K. Eibye, F. Marcello Iaia, J. Bangsbo, M. Hostrup, High-intensity exercise training enhances mitochondrial oxidative phosphorylation efficiency in a temperature-dependent manner in human skeletal muscle: Implications for exercise performance. *FASEB J.* **33**, 8976–8989 (2019).
101. G. P. Holloway, A. M. Holwerda, P. M. Miotto, M. L. Dirks, L. B. Verdijk, L. J. C. van Loon, Age-associated impairments in mitochondrial ADP sensitivity contribute to redox stress in senescent human skeletal muscle. *Cell Rep.* **22**, 2837–2848 (2018).
102. P. Schönfeld, L. Wojtczak, Fatty acids decrease mitochondrial generation of reactive oxygen species at the reverse electron transport but increase it at the forward transport. *Biochim. Biophys. Acta* **1767**, 1032–1040 (2007).
103. E. L. Robb, A. R. Hall, T. A. Prime, S. Eaton, M. Szibor, C. Viscomi, A. M. James, M. P. Murphy, Control of mitochondrial superoxide production by reverse electron transport at complex I. *J. Biol. Chem.* **293**, 9869–9879 (2018).
104. H.-S. Wong, B. Benoit, M. D. Brand, Mitochondrial and cytosolic sources of hydrogen peroxide in resting C2C12 myoblasts. *Free Radic. Biol. Med.* **130**, 140–150 (2019).
105. R. L. S. Goncalves, M. A. Watson, H. S. Wong, A. L. Orr, M. D. Brand, The use of site-specific suppressors to measure the relative contributions of different mitochondrial sites to skeletal muscle superoxide and hydrogen peroxide production. *Redox Biol.* **28**, 101341 (2020).
106. S. Larsen, N. Stride, M. Hey-Mogensen, C. N. Hansen, L. E. Bang, H. Bundgaard, L. B. Nielsen, J. W. Helge, F. Dela, Simvastatin effects on skeletal muscle: Relation to decreased mitochondrial function and glucose intolerance. *J. Am. Coll. Cardiol.* **61**, 44–53 (2013).
107. D. A. Kane, E. J. Anderson, J. W. Price, T. L. Woodlief, C.-T. Lin, B. T. Bikman, R. N. Cortright, P. D. Neufer, Metformin selectively attenuates mitochondrial H_2O_2 emission without affecting respiratory capacity in skeletal muscle of obese rats. *Free Radic. Biol. Med.* **49**, 1082–1087 (2010).
108. E. H. Yeung, C. Zhang, S. L. Mumford, A. Ye, M. Trevisan, L. Chen, R. W. Browne, J. Wactawski-Wende, E. F. Schisterman, Longitudinal study of insulin resistance and sex hormones over the menstrual cycle: The BioCycle study. *J. Clin. Endocrinol. Metab.* **95**, 5435–5442 (2010).
109. R. H. Hämäläinen, K. J. Ahlqvist, P. Ellonen, M. Lepistö, A. Logan, T. Otonkoski, M. P. Murphy, A. Suomalainen, mtDNA mutagenesis disrupts pluripotent stem cell function by altering redox signaling. *Cell Rep.* **11**, 1614–1624 (2015).
110. D. J. Fazakerley, R. Chaudhuri, P. Yang, G. J. Maghzal, K. C. Thomas, J. R. Krycer, S. J. Humphrey, B. L. Parker, K. H. Fisher-Wellman, C. C. Meoli, N. J. Hoffman, C. Diskin, J. G. Burchfield, M. J. Cowley, W. Kaplan, Z. Modrusan, G. Kolumam, J. Y. H. Yang, D. L. Chen, D. Samocha-Bonet, J. R. Greenfield, K. L. Hoehn, R. Stocker, D. E. James,

Mitochondrial CoQ deficiency is a common driver of mitochondrial oxidants and insulin resistance. *eLife* **7**, e32111 (2018).
111. M. L. Dirks, P. M. Miotto, G. H. Goossens, J. M. Senden, H. L. Petrick, J. van Kranenburg, L. J. C. van Loon, G. P. Holloway, Short-term bed rest-induced insulin resistance cannot be explained by increased mitochondrial H_2O_2 emission. *J. Physiol.* **598**, 123–137 (2020).
112. B. R. Pinho, A. I. Duarte, P. M. Canas, P. I. Moreira, M. P. Murphy, J. M. A. Oliveira, The interplay between redox signalling and proteostasis in neurodegeneration: In vivo effects of a mitochondria-targeted antioxidant in Huntington's disease mice. *Free Radic. Biol. Med.* **146**, 372–382 (2020).
113. S. Reagan-Shaw, M. Nihal, N. Ahmad, Dose translation from animal to human studies revisited. *FASEB J.* **22**, 659–661 (2008).
114. D. E. Steenberg, J. R. Hingst, J. B. Birk, A. Thorup, J. M. Kristensen, K. A. Sjøberg, B. Kiens, E. A. Richter, J. F. P. Wojtaszewski, A single bout of one-legged exercise to local exhaustion decreases insulin action in nonexercised muscle leading to decreased whole-body insulin action. *Diabetes* **69**, 578–590 (2020).
115. C. T. Putman, N. L. Jones, G. J. F. Heigenhauser, Effects of short-term training on plasma acid-base balance during incremental exercise in man. *J. Physiol.* **550**, 585–603 (2003).
116. M. I. Lindinger, L. L. Spriet, E. Hultman, T. Putman, R. S. McKelvie, L. C. Lands, N. L. Jones, G. J. F. Heigenhauser, Plasma volume and ion regulation during exercise after low- and high-carbohydrate diets. *Am. J. Physiol.* **266**, R1896–R1906 (1994).
117. O. Siggaard-Andersen, P. D. Wimberley, N. Fogh-Andersen, I. H. Gøthgen, Measured and derived quantities with modern pH and blood gas equipment: Calculation algorithms with 54 equations. *Scand. J. Clin. Lab. Invest.* **48**, 7–15 (1988).
118. F. Péronnet, D. Massicotte, Table of nonprotein respiratory quotient: An update. *Can. J. Sport Sci.* **16**, 23–29 (1991).
119. A. G. Cox, C. C. Winterbourn, M. B. Hampton, in *Measuring the Redox State of Cellular Peroxiredoxins by Immunoblotting. Thiol Redox Transitions in Cell Signaling, Part B* (Elsevier Inc., ed. 1, 2010), vol. 474, pp. 51–66.
120. A. M. James, H. M. Cochemé, R. A. J. Smith, M. P. Murphy, Interactions of mitochondria-targeted and untargeted ubiquinones with the mitochondrial respiratory chain and reactive oxygen species: Implications for the use of exogenous ubiquinones as therapies and experimental tools. *J. Biol. Chem.* **280**, 21295–21312 (2005).
121. N. Wijesekara, A. Tung, F. Thong, A. Klip, Muscle cell depolarization induces a gain in surface GLUT4 via reduced endocytosis independently of AMPK. *Am. J. Physiol. Endocrinol. Metab.* **290**, E1276–E1286 (2006).
122. A. Katz, S. S. Nambi, K. Mather, A. D. Baron, D. A. Follmann, G. Sullivan, M. J. Quon, Quantitative insulin sensitivity check index: A simple, accurate method for assessing insulin sensitivity in humans. *J. Clin. Endocrinal. Metab.* **85**, 2402–2410 (2000).
123. J. C. Levy, D. R. Matthews, M. P. Hermans, Correct homeostasis model assessment (HOMA) evaluation uses the computer program. *Diabetes Care* **21**, 2191–2192 (1998).

Acknowledgments: We thank all the study participants. We are grateful to J. J. Nielsen and M. Thomassen (August Krogh Section for Human Physiology, Department of Nutrition, Exercise and Sports at the University of Copenhagen) for technical support during the human experiments. We also thank M.P. Murphy (MRC Mitochondrial Biology Unit, University of Cambridge) for the quantification of mitoquinone content in skeletal muscle biopsy samples and MitoQ Limited for providing the mitoquinone and placebo capsules used in the human experiments. MitoQ Limited was not involved in the conceptualization and design of the study, data collection, data analysis and interpretation, or preparation of the manuscript. Figures were created with BioRender.com. **Funding:** This work was supported by Novo Nordisk Foundation grant NNF18OC0052883 (M.F. and J.B.) and Danish Diabetes Academy grant NNF17SA0031406 (J.O. and C.H.-O.). **Author contributions:** Conceptualization: M.F., M.H., and J.B. Methodology: M.F., J.O., C.H.-O., T.E.J., J.F.P.W., M.H., and J.B. Validation: M.F., T.E.J., and J.B. Formal analysis: M.F. Investigation: M.F., J.O., C.H.-O., K.W.P., S.A.H., and T.E.J. Resources: T.E.J. and J.F.P.W. Data curation: M.F. Writing—original draft: M.F. Writing—review and editing: M.F., J.O., C.H.-O., T.E.J., J.F.P.W., M.H., and J.B. Visualization: M.F. and C.H.-O. Supervision: T.E.J., J.F.P.W., M.H., and J.B. Project administration: M.F., T.E.J., M.H., and J.B. Funding acquisition: M.F., J.F.P.W., and J.B. All authors contributed to data interpretation, critically revised the manuscript for important intellectual content, and approved the final version of the manuscript. **Competing interests:** J.F.P.W. has ongoing collaborations with Pfizer Inc. and Novo Nordisk A/S unrelated to this study. J.F.P.W. holds shares in Novo Nordisk A/S and Pfizer Inc. All other authors declare that they have no competing interests. **Data and materials availability:** All data needed to evaluate the conclusions in the paper are present in the paper and/or the Supplementary Materials.

Submitted 17 May 2024
Accepted 23 September 2024
Published 30 October 2024
10.1126/sciadv.adq4461